



Contents lists available at ScienceDirect

Remote Sensing of Environment

journal homepage: www.elsevier.com/locate/rse

ESA's Soil Moisture and Ocean Salinity mission: From science to operational applications

S. Mecklenburg^{a,*}, M. Drusch^b, L. Kaleschke^c, N. Rodriguez-Fernandez^d, N. Reul^e, Y. Kerr^d, J. Font^f, M. Martin-Neira^b, R. Oliva^g, E. Daganzo-Eusebio^b, J.P. Grant^h, R. Sabiaⁱ, G. Macelloni^j, K. Rautiainen^k, J. Fauste^g, P. de Rosnay^l, J. Munoz-Sabater^l, N. Verhoest^m, H. Lievens^m, S. Delwart^a, R. Crapolicchio^a, A. de la Fuente^a, M. Kornberg^b

^a European Space Agency, ESA-ESRIN, Frascati, Italy

^b European Space Agency, ESA-ESTEC, Noordwijk, The Netherlands

^c University of Hamburg, Hamburg, Germany

^d CESBIO, Toulouse, France

^e Ifremer, Plouzané, France

^f ICM-CSIC & SMOS-BEC, Barcelona, Spain

^g European Space Agency, ESA-ESAC, Madrid, Spain

^h Consultant to ESA, Malmö, Sweden

ⁱ Telespazio-Vega UK Ltd for ESA, ESRIN, Frascati, Italy

^j IFAC, Florence, Italy

^k FMI, Helsinki, Finland

^l ECMWF, Reading, UK

^m Ghent University, Ghent, Belgium

ARTICLE INFO

Article history:

Received 5 August 2015

Received in revised form 2 December 2015

Accepted 17 December 2015

Available online xxx

Keywords:

Soil Moisture and Ocean Salinity (SMOS) mission

Sea surface salinity

Soil moisture

Sea ice thickness

Vegetation optical depth

Severe wind tracking

Data assimilation

Hydrological forecasting

L-band radiometry

Satellite remote sensing

Freeze and thaw

ABSTRACT

The Soil Moisture and Ocean Salinity (SMOS) mission, launched in November 2009, is the European Space Agency's (ESA) second Earth Explorer Opportunity mission. The scientific objectives of the SMOS mission directly respond to the need for global observations of soil moisture and ocean salinity, two key variables used in predictive hydrological, oceanographic and atmospheric models. SMOS observations also provide information on vegetation, in particular plant available water and water content in a canopy, drought index and flood risks, surface ocean winds in storms, freeze/thaw state and sea ice and its effect on ocean–atmosphere heat fluxes and dynamics affecting large-scale processes of the Earth's climate system.

Significant progress has been made over the course of the now 6-year life time of the SMOS mission in improving the ESA provided level 1 brightness temperature and level 2 soil moisture and sea surface salinity data products. The main emphasis of this paper is to review the status of the mission and provide an overview and performance assessment of SMOS data products, in particular with a view towards operational applications, and using SMOS products in data assimilation.

SMOS is in excellent technical condition with no limiting factors for operations beyond 2017. The instrument performance fulfils the requirements. The radio-frequency interference (RFI) contamination originates from man-made emitters on ground, operating in the protected L-band and adding signal to the natural radiation emitted by the Earth. RFI has been detected worldwide and has been significantly reduced in Europe and the Americas but remains a constraint in Asia and the Middle East. The mission's scientific objectives have been reached over land and are approaching the mission objectives over ocean.

This review paper aims to provide an introduction and synthesis to the papers published in this RSE special issue on SMOS.

© 2016 Elsevier Inc. All rights reserved.

1. Introduction

Being launched in November 2009, the Soil Moisture and Ocean Salinity (SMOS) mission is the European Space Agency's (ESA) second Earth Explorer Opportunity mission within its Living Planet Programme

* Corresponding author at: ESA-ESRIN, Via Galileo Galilei, 00044 Frascati, Italy.
E-mail address: susanne.mecklenburg@esa.int (S. Mecklenburg).

and has now been in orbit for 6 years. ESA and the Centre National d'Etudes Spatiales (CNES) jointly operate the SMOS mission.

SMOS was the first mission providing global measurements of L-band brightness temperatures resulting in soil moisture and ocean salinity data sets from space, directly responding to the lack of such measurements for hydrological and oceanographic applications (Kerr et al., 2010). Both these parameters are key variables within the Earth's water cycle and have been identified as Essential Climate Variables (ECVs) by the Global Climate Observing System (GCOS, Systematic observation requirements for satellite-based products for climate, WMO/TD No. 1338, GCOS-107, September 2006). The objectives of the SMOS mission respond directly to the scientific challenges outlined in the "Earth Observation Science Strategy for ESA" (http://esamultimedia.esa.int/multimedia/publications/SP-1329_1/offline/download.pdf) and are summarised in the "Mission Objectives and Scientific Requirements of the Soil Moisture and Ocean Salinity (SMOS) Mission (MRD)" (Kerr et al., 2001b, http://esamultimedia.esa.int/docs/SMOS_MRD_V5.pdf) as: (1) To provide global volumetric soil moisture estimates with an accuracy of $0.04 \text{ m}^3\text{m}^{-3}$ at a spatial resolution of 35–50 km and a temporal sampling of 1–3 days and (2) To provide global ocean salinity estimates with an accuracy of 0.1 practical salinity scale units (pss) for a 10–30 day average for an open ocean area of $200 \text{ km} \times 200 \text{ km}$. SMOS observations also provide valuable information on the characterisation of sea ice, soil freeze/thaw state as well as vegetation and thus enhance our understanding of the energy, water and carbon exchange processes between the Earth's surface and the atmosphere.

The payload of SMOS (Fig. 1) consists of the Microwave Imaging Radiometer using Aperture Synthesis (MIRAS) instrument, a passive microwave 2-D interferometric radiometer, operating in L-band (1.413 GHz, 21 cm wavelength) within the protected 1400–1427 MHz band. The interferometry technology has been developed for radioastronomy and provides the opportunity to measure at a spatial resolution suitable for the global measurements required (Kerr et al., 2001a). Interferometry is used to address the constraint (in space) that the antenna size is proportional to the wavelength and the spatial resolution achieved, hence synthetic aperture and interferometric processing are required for space applications addressing the Earth's water cycle. The technical concept used for SMOS is unique in that it has been applied in space, for an Earth Observation mission, for the first time. MIRAS comprises a central structure and three deployable arms holding the equally distributed 69 antenna elements. SMOS measures the brightness temperature emitted from the Earth at L-band over a range of incidence angles (0 to 55°) across a swath

of approximately 1000 km with a spatial resolution of 35 to 50 km. MIRAS has the functionality to provide measurements in dual and full polarisation, with the latter being the mode in which MIRAS is presently operated. For a detailed description of the MIRAS components see (McMullan et al., 2008), for an assessment of the MIRAS performance in orbit see (Martin-Neira et al., 2015).

The SMOS mission is based on a sun-synchronous orbit (dusk-dawn 6 am/6 pm) with a mean altitude of 758 km and an inclination of 98.44° . SMOS has a 149-day repeat cycle with an 18-day sub-cycle and a revisit time of 3 days at the equator.

Measurements in L-band are a new observation type for scientific and operational user communities. They allow accurate global observations of emitted radiation originating from land and ocean surfaces since the atmosphere is almost transparent in this spectral range. The sensitivity to changes of the water content in the soil and the salinity in the oceans is high for low microwave frequencies when compared to measurements at higher frequencies provided through operational sensors, e.g. the Special Sensor Microwave Imager (SSM/I). The all-weather-all-surfaces capabilities address the needs of a large range of user communities and applications.

SMOS was the first interferometric satellite mission operating in the protected passive band 1400–1427 MHz. Nevertheless strong interference sources have been detected worldwide though the situation is continuously improving (Oliva et al., 2012a and Oliva et al., 2015; Daganzo-Eusebio et al., 2013).

Three dedicated (passive) L-band missions, namely ESA's SMOS (2009–) (Kerr et al., 2010; Mecklenburg et al., 2012), NASA's Aquarius (2011–2015) (Lagerloef et al., 2013; Le Vine et al., 2014), and SMAP (2015–) (Entekhabi et al., 2011, Brown et al., 2013) missions, have provided or still provide global measurements of brightness temperatures. Even though SMOS, Aquarius and SMAP all operate in the same spectral region, L-band, they differ in technology, spatial and temporal resolution, bandwidth, measurement accuracy and availability of ancillary data. Whereas SMOS was designed to provide data for both ocean salinity and soil moisture, Aquarius and SMAP focus on only one of those products. All three missions are characterised by different requirements and feature different measurement techniques. The uniqueness of the SMOS mission concept (compared to SMAP and Aquarius) is the multi-angular viewing capability allowing for i) the simultaneous retrieval of soil moisture and vegetation optical depth over land and ii) partially decoupling sea surface salinity and roughness signatures over ocean. Compared to Aquarius, SMOS offers an improved spatial and temporal resolution for the salinity data product. Both the Aquarius and SMAP missions combine a passive microwave sensor with an active L-band radar, to either correct the impact of the surface roughness in the observations over ocean for improved sea surface salinity retrievals (Aquarius) or to gain a higher spatial resolution for soil moisture observations (SMAP). Consequently, the three missions provide complementary data sets and scientific and operational applications benefit from their synergistic use. Thanks to their temporal sequence in being launched, merged data sets will become available covering approximately the decade from 2010 to 2020. Efforts have already been made to derive long-term global soil moisture datasets from passive microwave observations in preparation for their inclusion into ESA's Climate Change Initiative Project on Soil Moisture, focussing at present on merging AMSR-E and SMOS data (Al-Yaari et al., 2015; Van der Schalie et al., 2015, Rodriguez-Fernandez et al., 2015c).

Thanks to its excellent technical and scientific status (see Section 3) both ESA and the French Space Agency CNES, jointly operating the SMOS mission, have granted an extension to the SMOS mission operations until 2017. Currently there are no technical limitations to extend the mission operations beyond 2017.

Extending the mission operations, and hence the availability of observation data for longer time periods, enables the synergistic exploitation of SMOS data products with future observational data which will



Fig. 1. The SMOS mission – artistic view (ESA/AOES Medialab).

become available only during mission extension (e.g. ESA's Sentinel missions). It will also allow for enhanced process understanding of phenomena with time-scales exceeding the initial mission lifetime, in studying seasonal to inter-annual differences of large-amplitude signals and climate indices, such as e.g. El Nino and La Nina signals in sea surface salinity (Hasson et al., 2014), drought pattern monitoring (Al Bitar et al., 2013), generation of harmonised multi-mission data sets for climate monitoring etc. To address this point a new mission objective was added for the mission extension, namely that SMOS brightness temperatures, soil moisture, and ocean salinity observations shall be analysed with respect to geophysical processes related to the water cycle occurring on time scales exceeding the expected mission lifetime of 5 years.

Soil moisture, ocean salinity, and sea ice have been identified as Essential Climate Variables, with a clear need for long-term data series for such measurements. The most recent Intergovernmental Panel on Climate Change (IPCC) report (<http://www.ipcc.ch/report/ar5/>) released in September 2013 lists ocean salinity as a valuable monitoring tool to identify changes in regional to large scale oceanographic phenomena. Over land soil moisture can be used to monitor extreme weather and climate events. SMOS data can contribute to gather evidence in areas identified with low-medium confidence by IPCC, such as heat waves, droughts and tropical cyclone activity. Sea ice data products based on SMOS measurements can provide further evidence for the decrease in Arctic sea ice volume. The extent by which the Northern Hemisphere's snow cover decreases since the mid-20th century and the increase of permafrost temperatures in most regions since the early 1980s can be observed through soil frost data based on SMOS observations.

In continuing the provision of observation data sets, the extension of the SMOS mission operations also provides the pre-requisite for developing (pre-) operational applications and establishing their use with operational users. SMOS data have significant potential for operational applications, as discussed in Section 4, which is also recognisable in

the fact that for the extension phase a new mission objective has been added, namely that daily sea ice thickness estimates based on SMOS observations shall be provided for the Northern Hemisphere with a spatial resolution of 10,000 km² up to maximum values of 50 cm.

Section 2 will give an overview on the technical status of the mission, the instrument performance, status of RFI and the scientific products and their verification. Section 3 focusses on product evolution, introducing newly developed and future SMOS data products as well as the use of SMOS data products in data assimilation. Section 4 provides a summary and outlook on future work.

2. SMOS after 6 years in orbit

2.1. Mission status

SMOS was developed in collaboration with the French Space Agency CNES, and the Spanish Centro para el Desarrollo Tecnológico Industrial (CDTI). This collaborative approach continues in the operations phase: ESA is responsible for the overall mission, instrument and ground segment operations whereas CNES is responsible for the operations of the satellite platform PROTEUS.

The SMOS space segment, comprising the PROTEUS platform and the MIRAS instrument, is fully operational with no sign of degradation. Fig. 2 shows the amount of degraded and lost data over the mission lifetime and confirms that the availability of observation data is well within the system performance requirement of 98%. Some well-identified anomalies with their respective recovery procedures are in place with no major impact on the availability of science data. The anomalies are assumed to be driven mostly by a high radiation environment. They mainly affect the Control and Correlation Unit (CCU), being the central computer, the Control and Monitoring Nodes (CMN), one per arm segment handling commands from and telemetry to the CCU, and the mass memory.

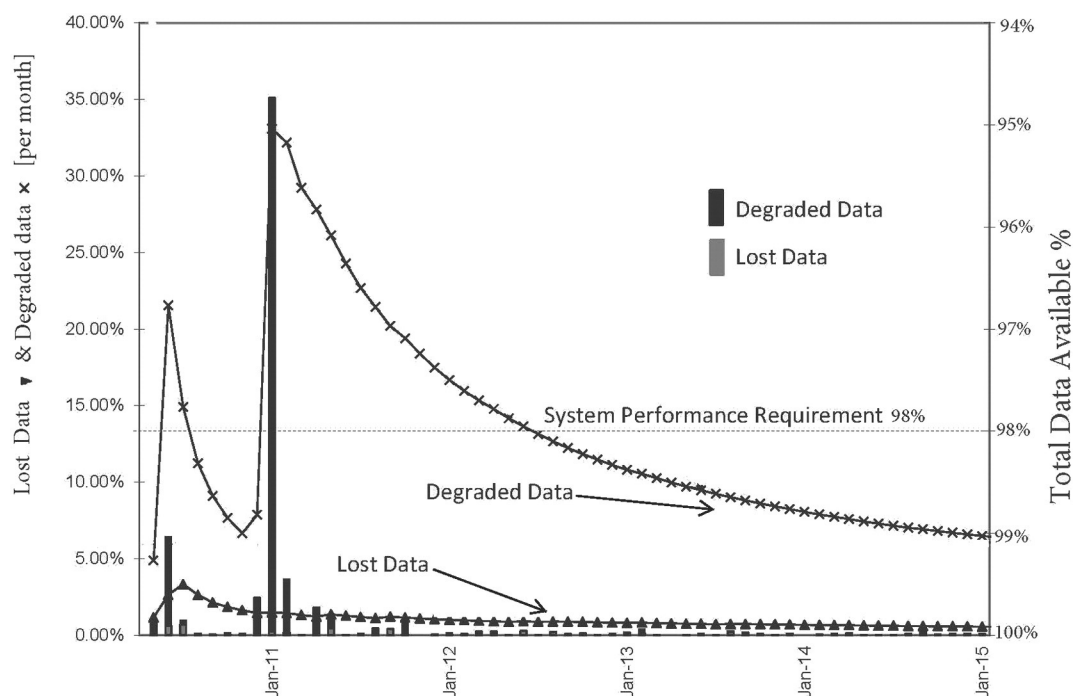


Fig. 2. Availability of observation data from SMOS remains high at approximately 98%. For example, the cumulative data lost since 1 May 2010 amounts to 0.08% and the degraded data amount to 0.94% (status: March 2015).

Table 1
SMOS calibration activities in the operations phase.

Calibration activity	What it does	Impact on data availability
Flat target acquisition (6 months)	Measurement of flat target response (antenna errors)	0.038%
Long calibration (8 weeks)	Measurement of receiver gain and offset and correlator errors	0.132%
Cold sky calibration (2 weeks)	Measurement of noise injection radiometer gain-offset and antenna losses	0.496%
Short calibration (1 week)	Measurement of receiver offset	0.017%
Local oscillator (10 min)	Measurement of local oscillator phase	1%
	Total of time spent on calibration activities on acquired data	1.68%

Extrapolating from current consumption, sufficient propellant for more than 120 years in orbit is available thanks to a very precise injection into orbit at launch and minimal consumption in operations, which is limited to orbit correction (approximately every 3 months) and collision avoidance manoeuvres (10 since beginning of the mission, status May 2015).

The ground segment acquires, processes and disseminates data products up to level 2. Due to the availability of two ground stations at ESA-ESAC near Madrid (Spain) and Svalbard (Norway) no data is lost in acquisition. The data production is successfully completed in approximately 99% for all data products provided by ESA. ESA also provides level 1 brightness temperature data in near-real time (NRT) to operational agencies, being available within 3 h from sensing in 90% of the time. NRT data are available either directly from ESA or from the WMO's Global Telecommunication System (GTS) network, with the UK Met Office injecting the data into the system, as well as from EUMETSAT's EUMETCast system.

2.2. Instrument performance and calibration

To ensure the quality of observation data a sequence of calibration activities is regularly performed and takes up 1.68% of the acquisition time (Mecklenburg et al., 2012). The calibration strategy for SMOS, defined at the end of the commissioning phase in 2010, has remained stable throughout the operations (Table 1), with minor adjustments. In 2012 short calibrations were introduced in between long calibrations for more frequent measurements of the receiver offset. In 2014 the ambient conditions for the cold sky calibrations were adjusted to reduce thermal related problems observed in some of the antenna receivers (the LICEFs). The Noise Injection Radiometer (NIR) calibrations are now performed with the Sun in front of the antenna plane at an elevation not exceeding 10°. This ensures higher temperatures at the instrument, which are closer to the thermal behaviour during actual measurements.

Table 2
SMOS instrument performance, status: June 2015. Specified and measured values are given as root mean square error of brightness temperatures in Kelvin [K rms]. B stands for boresight, E for edge of swath, AF for Alias Free Field of View, EAF for Extended Alias Free Field of View. Sky, ocean and Antarctica refers to type of surface over which the measurements have been made.

System parameter	Specified value	Measured value (in-orbit)
Systematic error	1.5 K rms (B)	0.57 K rms (AF, sky)
	2.5 K rms (E)	2.3 K rms (EAF, ocean)
Level 1 soil moisture radiometric sensitivity (1.2 s–220 K)	3.5 K rms (B)	2.5 K rms (B, Antarctica)
	5.8 K rms (E)	4.0 K rms (E, Antarctica)
Level 1 ocean salinity radiometric sensitivity (1.2 s–150 K)	2.5 K rms (B)	2.0 K rms (B, ocean)
	4.1 K rms (E)	2.5 K rms (E, ocean)
Pointing	400 m	221 m (ascending orbit)
		388 m (descending orbit)

Table 2 summarises the main instrument performance parameters, all being within specification. While the radiometric resolution, set by fixed instrument parameters and integration time, has remained the same since the beginning of the mission, systematic errors have been reduced by about 30% through several calibration and image reconstruction improvements, and pointing has been refined using ground interferers-of-opportunity at known locations.

Table 3 summarises the improvements achieved for stability and drift for the currently deployed level 1 processor v6 (Martin-Neira et al., 2015) providing brightness temperatures. The long-term stability of the measured brightness temperatures both over ocean and Antarctica has been improved substantially. Instrument calibration drifts have largely been compensated for and much of the seasonal trend over the ocean has been removed. The improvements at both annual and seasonal scales have mainly been achieved by introducing a more accurate calibration of the losses of the antenna. Orbital biases (ascending versus descending) were reduced with some non-optimal performances at high latitudes during the eclipse period (November to January) remaining. Instrumental spatial biases have been reduced but not to the level that would allow removing the Ocean Target Transformation (OTT) (Font et al., 2013) correction, necessary for the sea surface salinity retrieval. The so-called land-sea contamination effect, the leakage of the signal coming from land into ocean preventing reliable salinity retrieval along the coastlines, is still present in the level 1 v6 processor, mainly impacting marine applications near the coast.

Besides the routine instrument calibration, external targets have been used to calibrate and validate SMOS observations. For higher brightness temperature values (i.e. higher than 150 K) the Antarctic plateau is suitable as a calibration site due to its slow changing environment and physical structure of the polar ice sheet. In particular the region around Dome-C in East Antarctica, with the permanent Italian-French base Concordia, has been used for comparisons between ground and space based observations. Several studies have been performed to investigate the spatial variability and temporal stability of this area. Observations acquired by a ground based L-band radiometer (RADOMEX) located at Dome-C, prove the high temporal stability of this area throughout the year with brightness temperatures in V-polarisation varying less than 1 K (Macelloni et al., 2012, Macelloni et al., 2013 and Macelloni et al., 2014). In H-polarisation data showed a higher variation with a standard deviation of approximately 1.5 K (Macelloni et al., 2006 and Macelloni

Table 3
Summary of improvements for stability and drift in the currently deployed level 1 v6 processor compared to previous processor version v5 for 1st Stokes parameter $(T_x + T_y)/2$.

$(T_x + T_y)/2$	Previous level 1 (V5)	Current level 1 (V6)
Orbital stability, latitudinal slope	6.9 mK/lat deg	4 mK/lat deg
Seasonal stability	0.38 K	0.16 K
Long term stability: yearly drift	−0.18 K/year	−0.03 K/year

Table 4

Global mean statistics (after bias correction, considering xx and yy pol and 30, 40, 50 degree incidence angles) comparing SMOS (v5) with CMEM brightness temperatures from the re-analysis data for 2010–2013.

Year	RMSE (K)	R	Anomaly R
2010	8.64	0.598	0.293
2011	7.99	0.615	0.302
2012	7.70	0.627	0.318
2013	7.34	0.647	0.332

et al., 2013), which is consistent with results obtained at higher frequencies (Picard et al., 2009; Macelloni et al., 2007) and due to the fact that H-polarisation is more sensitive to modification of snow-pack layering and surface properties. An airborne campaign over DOME-C performed in 2013, called DOMEair, observed brightness temperature variations of several Kelvin across a 350 km cross section (Skou et al., 2015). SMOS observations display similar features but, given the size of the SMOS footprint, smaller scale inhomogeneities are smoothed out. In addition, the temporal variability of SMOS observations is small, with an annual variability of the brightness temperatures of approximately 1 K at V-polarisation and 2 K at H-polarisation. However, the airborne results point out that care should be taken when choosing footprints as a calibration reference.

ECMWF provides continuous performance monitoring of SMOS observations globally over land and ocean as well as over targeted measurement sites (http://old.ecmwf.int/products/forecasts/d/charts/monitoring/satellite/smos/o_smos_smos_histland/). For the development of the bias correction, re-analysis data and the Community Microwave Emission Modelling Platform (CMEM) (e.g. Drusch et al., 2009, De Rosnay et al., 2009) have been used to compute a consistent and stable model based brightness temperature data set. Table 4 shows the global mean statistics for the comparison of observed SMOS brightness temperatures with the simulated CMEM re-analysis data set, displaying a consistent improvement from 2010 to 2013. Although there are uncertainties in both the observations and the model simulations, these statistics are based on the comparison between the SMOS reprocessed data and the ECMWF re-analysis forward brightness temperatures. So, the simulated and the observed brightness temperature rely on consistent versions of the model and processor, respectively. Improvements in statistics can be attributed to an improved SMOS data quality, with the CMEM model and the re-analysis data being stable over the 4-year time period, likely due to improved RFI situation globally and more refined RFI flagging (Section 3.3). A detailed discussion will be provided in (De Rosnay et al., 2015).

2.3. Radio-frequency interference

SMOS was the first interferometric satellite mission operating in the Earth Exploration Satellite Service (EESS) passive band 1400–1427 MHz, in which all emissions are prohibited according to the International Telecommunication Union (ITU) Radio-Regulations, under the provision No. RR 5.340. Furthermore, ITU Resolution 750 urges administrations to ensure that unwanted emissions of active service stations in the bands 1350–1400 MHz and 1427–1452 MHz do not exceed the recommended maximum levels. Despite this regulatory frame extensive radio-frequency interference (RFI) are detected worldwide within the purely passive band 1400–1427 MHz (here after called “L-band”). The RFI are due either to stations operating within the passive band, or stations operating in the adjacent bands with excessive out-of-band emission levels.

The RFI sources originate from man-made emissions. An indication of the RFI strength is given by its brightness temperature, which

depends on the physical temperature of the scene and on the emissivity of the terrain/ocean. Typically any brightness temperature measurement over ground that exceeds 350 K is considered an RFI, however a more careful RFI detection requires the adjustment of brightness temperature thresholds depending on the observed region and season. RFI disturbs the natural microwave emission rendering the satellite observations in some cases unusable for retrieving SMOS data products in its presence. Naturally occurring radiation emitted by the Earth is very low (up to 350 K) compared to the active signal added by these emitters (ranging up to 10,000 K and higher in places). Low levels of RFI (i.e. within the natural occurrence up to 350 K) added to the signal will cause difficulties in distinguishing between natural and man-made radiations and will have a strong impact on the overall data quality and interpretation of the measurements (Report ITU-R RS.2178, 2010, Oliva et al., 2015).

Since launch RFI has impacted SMOS data products particularly over Europe, Asia and the Middle East (Oliva et al., 2012a; Daganzo-Eusebio et al., 2013). The RFI situation is continuously monitored worldwide and regular maps of RFI probability are provided to the science community. The concerted effort from ESA and the SMOS scientists has much improved the overall RFI scenario with 850 RFI sources being detected worldwide and 478 of these RFI sources (58%) being identified and not operating anymore in the protected band (status July 2015) (Oliva et al., 2015). Despite new RFI sources continuously coming on, they have, in general, been significantly reduced over the mission time span in particular over Europe and America (Fig. 3), but prevail in Asia and the Middle East. Reducing unwanted emissions has an immediate positive impact on SMOS data. Fig. 4 shows improved sea surface

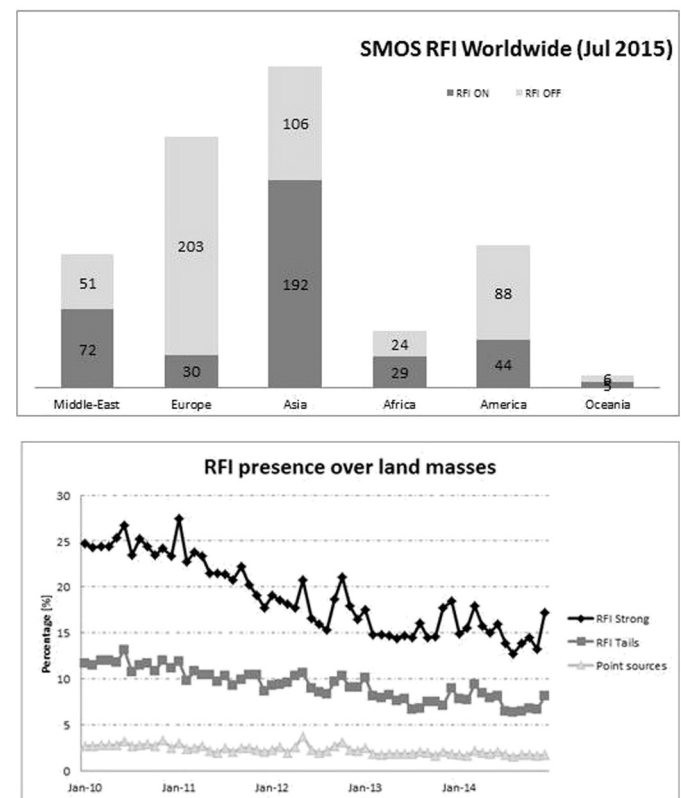


Fig. 3. Top: statistics of switched off and active RFI sources as seen by SMOS worldwide (Status: July 2015). Significant improvements have been made over Europe and America. Bottom: Percentage of the number of SMOS pixels over land affected by RFI for 2010–2014. Pixels flagged with strong RFI have decreased by 11% over the mission life time due to successfully switching off strong sources.

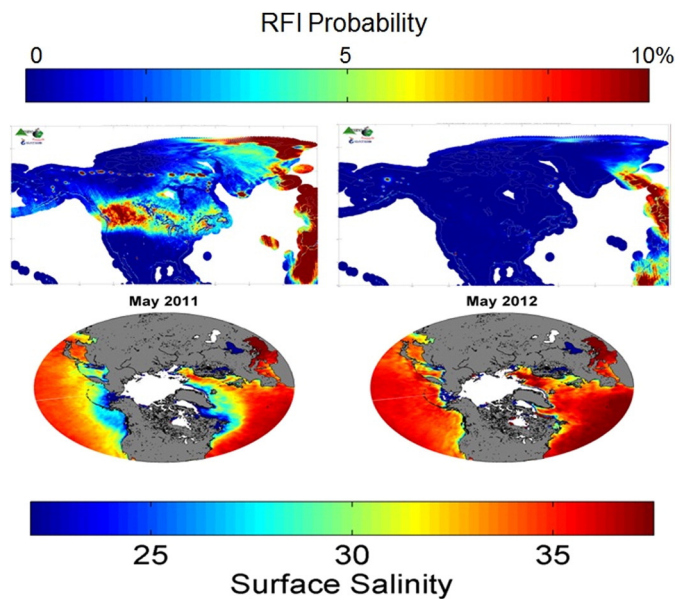


Fig. 4. Top: RFI probability map over North America, showing improvements due to the refurbishment of L-band radar stations between 2010 and 2012. Bottom: The reduction of RFI has led to improved sea surface salinity retrievals in Northern latitudes. May 2011 sees an unrealistic halo of fresh sea surface salinity values (in psu) around the coasts of Northern America due to unnatural high brightness temperatures induced by RFI, whereas May 2012 displays naturally expected sea surface salinity values after reducing RFI contamination.

salinity retrievals in the Northern latitudes after reducing RFI contamination in North America.

A pre-requisite to successfully suppressing RFI sources is precisely locating their position. The current algorithms locate RFI sources with an accuracy of only a few kilometres (Oliva et al., 2013) to a few hundred metres (Anterrieu et al., 2015). The RFI scenario has greatly improved worldwide due to the regular reporting of the RFI sources to over 50 national spectrum management authorities. As part of this reporting, ESA asks for their cooperation in investigating and taking remedial actions to eliminate the harmful interference on their territory. In case the administrations do not cooperate, the ESA may ask the ITU

Radiocommunication Bureau (BR) for assistance to solve the case. Fig. 3 shows the successful reduction of the strongest emissions by half over the mission life time.

Improvements to the regulatory framework have been achieved within the European Conference of Postal and Telecommunications (CEPT) and also within the ITU. The ESA Frequency Management Office has had an active role in this process. The Electronic Communications Committee (ECC) at the CEPT approved a Decision of 11 March 2011 (ECC/DEC/(11)01) that translated the maximum recommended levels of unwanted emissions from the adjacent bands into mandatory levels. This ECC decision intends to provide a clear message towards reaching long term EESS (passive) protection and it has already been implemented in 17 European countries (status July 2015) (http://www.erodocdb.dk/doks/implement_doc_admin.aspx?docid=2398). A new ITU question ITU-R 255/7 (approved in May 2014) is now being addressed by the ITU study group 7C with the purpose to study and improve the reporting and resolution of RFI to EESS (passive) sensors.

In cases where RFI sources cannot be switched off RFI sources need to be detected and flagged accordingly. RFI filtering methods are continuously improved and evolved from the previously used simple threshold algorithm where brightness temperatures exceeding 340 K were masked as RFI. The current level 1 (v6) processor includes an improved RFI filtering approach using the instrument imaging characteristics and deviations from the nominal temporal behaviour of the antenna zero baselines to identify RFI sources (Anterrieu, 2011). The current level 2 (v6) processors use a statistical approach to detect RFI (Oliva et al., 2015), applying a threshold to the measured brightness temperatures and comparing it to the surface emissivity model derived values.

2.4. Scientific products and their verification

The retrieval algorithms for the SMOS level 2 scientific products for soil moisture and sea surface salinity (Fig. 5) are well described in Kerr et al. (2012); Boutin et al. (2012) and Font et al. (2010). Both rely on iterative convergence schemes that retrieve the geophysical products minimising the differences between SMOS observed and modelled brightness temperatures within a cost function, exploiting as well a-priori information on specific auxiliary data.

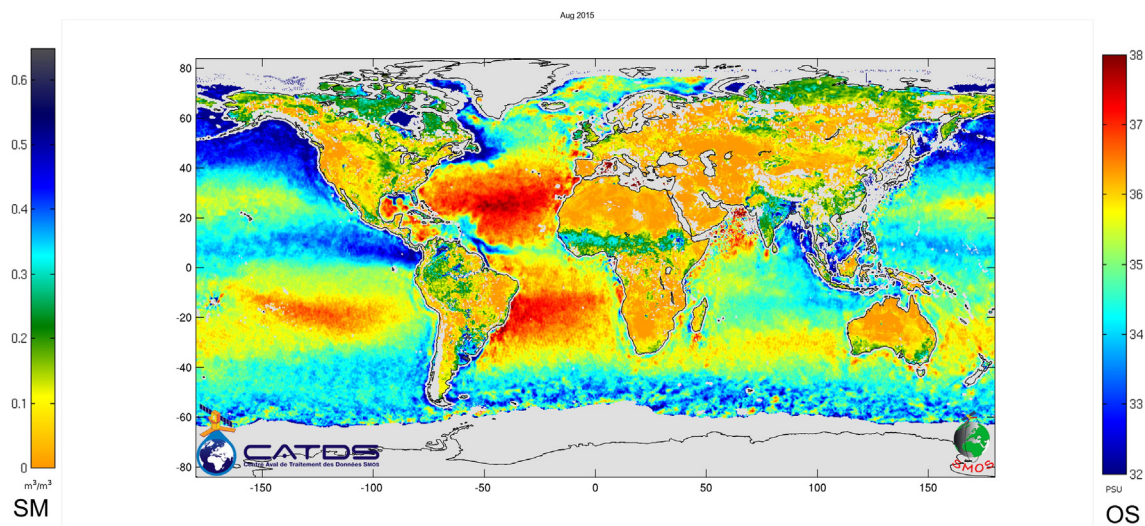


Fig. 5. Global map of SMOS derived soil moisture and sea surface salinity data for August 2015, level 2 processor version 6.

The current level 2 soil moisture processor (v6) better characterises diurnal effects than version v5 by splitting the values of vegetation optical depth, surface roughness and RFI probability between ascending and descending orbits. The auxiliary data files have also been improved in terms of their spatial resolution and/or quality, improved soil type characterisation and snow cover map. Finally the algorithm improves the soil moisture retrieval in forested areas and the RFI detection and flagging (Kerr et al., 2015; Oliva et al., 2015).

The current level 2 sea surface salinity processor (v6) optimises the use of the Vertical Total Electron Content (VTEC) (Vergely et al., 2014) in the retrieval and improves the detection and flagging of RFI (Reul et al., 2015a). Besides, it reduces the salinity bias by changing the OTT, an instrumental bias mitigation correction, computation and frequency and improves the data quality with refined roughness models and improved Sun and galactic noise flagging.

The performance of the retrieval and the data product accuracy at level 2 are continuously assessed through standard validation protocols. Soil moisture data are validated using in-situ observations from selected match-up sites, representing a variety of different biomes, and observations collected and quality controlled from the International Soil Moisture Network (Dorigo et al., 2013). Consistency checks and comparisons against modelled soil moisture fields from ECMWF's Integrated Forecasting System or different re-analyses are performed regularly. Sea surface salinity data are verified using a variety of in-situ data over several match-up sites (e.g. in the Tropics or the North Atlantic region corresponding to the sea surface salinity maximum) representative of various oceanographic conditions and regimes, including drifters, profilers, moored buoys and Research Vessel thermosalinographs, having differing sampling depths. The routine validation is carried out using optimally-interpolated in-situ observations from the upper 10 m of the oceans, as provided by the extensive Argo float network (Gaillard, 2012).

A specific protocol of data filtering, collocation and spatio-temporal binning is used to routinely perform these verifications, thus assessing the performances and their improvements between subsequent processor versions using a pre-defined metrics.

Over land, the mission objective, namely to provide global volumetric soil moisture estimates with an accuracy of $0.04 \text{ m}^3 \text{ m}^{-3}$ at a spatial resolution of 35–50 km and a temporal sampling of 1–3 days over nominal surfaces, has been met (Kerr et al., 2015). Over ocean, the mission objective (being very challenging given the limited dynamic range of brightness temperature over ocean), namely to provide global ocean salinity estimates with an accuracy of 0.1 pss units for a 10–30 day average for an open ocean area of $200 \text{ km} \times 200 \text{ km}$, has not yet been met globally. However, in most regions of the ocean within 45°S – 45°N , with a sea surface temperature higher than $\sim 10^\circ \text{C}$, it has nearly been accomplished when removing seasonal systematic errors at large scale (Hernandez et al., 2014; Reul et al., 2015a). It has to be noted, however, that these requirements were defined prior to the advent of the Argo float measurements, whose coverage of the ocean currently provides a very good monitoring of large scale ($>300 \text{ km}$) features; SMOS, in turn, has proven capabilities to detect mesoscale features not resolved by Argo, and recent studies have shown that a variability $>0.1 \text{ pss}$ may exist at scales $<300 \text{ km}$ (Reul et al., 2014a; Kolodziejczyk et al., 2015), questioning the prescribed accuracy requirements.

In general, SMOS is actually sensing geophysical signals at vertical and horizontal scales not resolved by in-situ data. This mismatch in information content results in additional (systematic) differences, which must not mistakenly be deemed measurement errors. Regional variations in data quality also occur due to RFI and land-sea contamination. A detailed performance assessment for the SMOS level 2 scientific products for soil moisture and sea surface salinity will be given in Kerr et al. and Reul et al. (both 2015).

3. Product evolution – towards operational applications

3.1. New products

After more than five years in orbit the catalogue of SMOS products is steadily increasing. In addition to the already available validated operational products (see Sections 2.2 and 2.4) new SMOS data products keep emerging and are in varying stages of implementation. For a summary of products see Table 5.

3.1.1. Sea ice thickness

Even though not being designed explicitly for cryospheric applications, SMOS brightness temperatures have become valuable for observing sea ice. Passive microwave sensors provide information about the sea ice cover without the limitation of clouds or the absence of sunlight during the long polar night, which prevents the observation in the visible range of the electromagnetic spectrum. Microwave imaging sensors operating in shorter wavelengths than L-band have regularly been used to derive the sea ice extent and concentration since the beginning of the 1970s. L-band radiometry is unique in comparison with previous sensors because the microwave emission measured at the satellite originates from deep ice layers. The emission depth depends on the dielectric absorption of the media and thus on ice salinity and temperature. The resulting sensitivity allows retrieving the sea ice thickness up to about 0.5–1.5 m, which is an important geophysical parameter for many applications. The uncertainty of the retrieval is in the order of 5–20% for young ice ($<30 \text{ cm}$) and increases with increasing thickness.

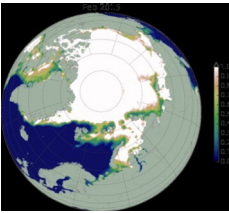
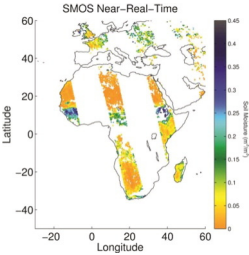
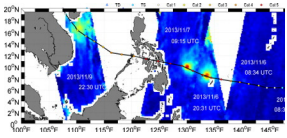
SMOS provides a daily coverage of the Arctic sea ice up to about 87°N thanks to its inclination of 98.44° . However, the retrieval is restricted to cold seasons (October–April in the Northern Hemisphere) because the L-band penetration depth decreases with increasing ice temperature and melting conditions strongly limit the retrieval capability. The current operational retrieval is based on a combined sea ice thermodynamic and emissivity model accounting for ice temperature and ice salinity (Kaleschke et al., 2012; Tian-Kunze et al., 2014). Daily maps and SMOS sea ice data products for the Arctic are available from <http://icdc.zmaw.de>, disseminated with a latency of approximately 24 h. A SMOS sea ice thickness product for the Antarctic is under development.

Average SMOS derived sea ice thickness data for February and March from 2011 to 2015 are shown in Fig. 6. Sea ice thickness observations and their assimilation in forecast models are important for short-range up to seasonal predictions (Yang et al., 2014; Day et al., 2014). Accurate measurements of the thin ice coverage are not available from other satellite sensors, which makes SMOS a unique component of the Arctic observing system.

In addition to validation campaigns performed over the Baltic Sea (Kaleschke et al., 2010; Maaß et al., 2015), recently carried out validation campaigns in the Arctic have provided the necessary ground truth to assess the performance of this data product and quantify the uncertainties associated. The comparisons of the SMOS sea ice thickness product with collocated data from an airborne laser scanner confirm the validity of the SMOS retrieval within the range of uncertainty as given in the SMOS product. The data from a linear swath laser scanner installed in the research aircraft Polar-5 of the Alfred-Wegener-Institute (AWI) can be considered as truly independent because the thickness is derived from the ice freeboard with assumptions about the density of ice and snow and the snow thickness (Kaleschke et al., 2015b). The sea ice dynamics in the Barents Sea generated a zone of heavy deformation east of the island of Edgeøya (Fig. 7). This pattern of thick ice is well represented in the SMOS data.

Recent efforts have focused on providing a synergistic ice thickness product combining the complementary skill from ESA's SMOS and CryoSat-2 missions. Both missions are complementary in the data they

Table 5
Summary of characteristics for new operational SMOS products on sea ice thickness, soil moisture in NRT and severe wind speed.

Data product	Sea ice thickness	Soil moisture in NRT	Severe winds
Operational implementation	Implemented, available since September 2014	In development, available from 2016 onwards	In preparation, implementation TBC
Reference for retrieval algorithm	Tian-Kunze et al. (2014), Kaleschke et al. (2012)	Rodríguez-Fernández et al. (2015a) and Rodríguez-Fernández et al. (2015b)	Reul et al. (2012), Reul et al. (2015b)
Input data	SMOS brightness temperatures	SMOS brightness temperatures in NRT	SMOS brightness temperatures
Spatial resolution	Product gridded into 12.5 km NSIDC polar stereographic projection (SMOS input data at 35–50 km)	Product provided in 15 km on ISEA 4H9 grid on slightly reduced swath (914 km) compared to ESA level 2 soil moisture product (1000 km)	Product provided at 15 km on a Mercator grid.
Latency	Daily maps, 24 h	Within 3 h from sensing	TBC
Dynamic range	up to 0.5–1.5 m with accuracy of ~5–10 cm for thin ice (<50 cm)	As ESA level 2 soil moisture data product	Up to 70–80 m/s with accuracy of ~5 m/s
Complementary products from [sensors]	CryoSat2, MODIS, SSM/I, AMSR-E		<ul style="list-style-type: none"> • GFDL model predicted wind fields • H*WIND NOAA/HRD analyses • NOAA/SFMR • Scatterometer (ASCAT) • WindSat (C-Band)
Advantage compared to other sensors	Provides daily coverage, independent of atmospheric conditions (clouds/MODIS), large sensitivity to thin sea ice	Neural network trained on geophysical product, fast algorithm	Negligible impact of atmospheric effects, rain and sea spray on emission signal; Scatterometer data saturate at U ~ 33 m/s (Hurricane force)
Validation	Comparison to airborne electromagnetic induction (EM) and laser scanner instrument. Comparison to thin ice thickness derived from MODIS thermal infrared method, CryoSat2 altimetry and ocean-ice model assimilation systems TOPAZ and PIOMAS.	Comparison to in-situ measurements from over 1000 stations worldwide (Rodríguez-Fernández et al., 2015b). Similar or better statistics than the ESA level 2 soil moisture data product.	Good agreement with airborne measurements: SFMR C-Band; Good agreement with H*WIND and (when available) buoy anemometers
Uncertainties	See Table 1 in Tian-Kunze et al. (2014): uncertainties for ice thickness between 0 and <50 cm in function of fixed std (Tb) = 0.5 K, std (Tice) = 1 K and std (Sice) = 1 g kg ⁻¹ vary between few cm to 1 m exponentially; for thin ice up to 10 cm uncertainties are less than 1 cm, for ice thickness up to 50 cm max uncertainty is 22 cm, for ice thickness more than 50 cm uncertainties vary between 4 cm up to 1 m.	Slight underestimation (up to 0.04 m ³ /m ³) for high values of soil moisture with respect to the ESA level 2 soil moisture data product	Uncertainties are in the order of 5 m/s for wind speeds up to 70–80 m/s. These residual errors can be due to potential sea state effects, presence of ice cloud and extremely high rain rates.
Provider/available from	University of Hamburg, http://icdc.zmaw.de	ESA Once released available from EUMETCast and GTS (for details see https://earth.esa.int/web/guest/-/how-to-obtain-data-7329)	IFREMER http://www.smosstorm.org/
Product format	NETCDF	NETCDF	NETCDF
Available for/since	Product available for Northern hemispheric winter season (October to April), from 2010 till now	Global, all year, from 2010 till now	Global, all year, from 2010 till now
Sample product	 Monthly sea-ice thickness over the Arctic Ocean. Credits University of Hamburg, ESA.	 Soil Moisture data product in near-real-time (NRT). Credits CESBIO, ESA.	 SMOS retrieved surface wind speed [km/h] along the eye track of super typhoon Haiyan from 4 to 9 November 2013. Credits: IFREMER, ESA.

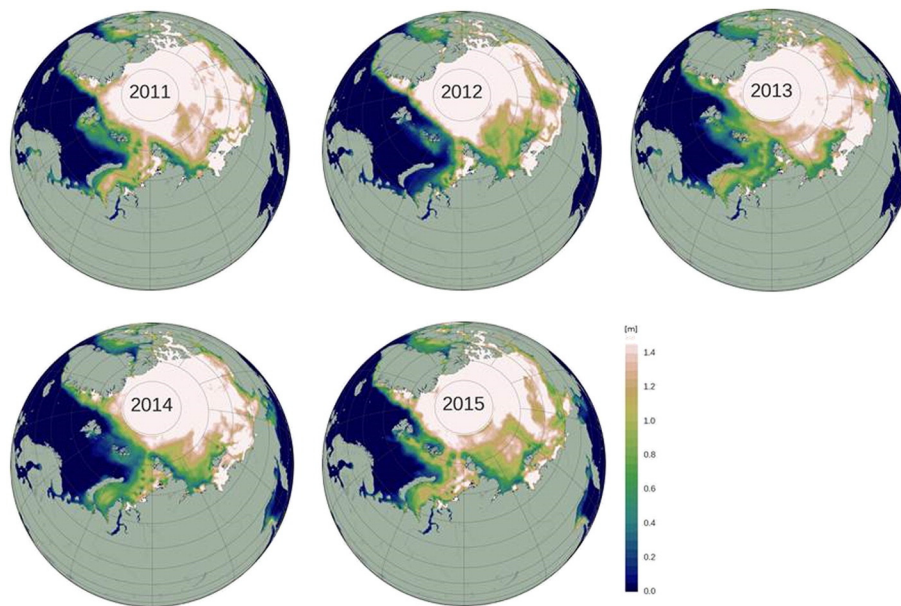


Fig. 6. SMOS derived sea ice thickness for February and March (average) from 2011 to 2015 in [m].
Credit: University of Hamburg, ESA.

provide and their error characteristics. CryoSat-2, using altimetry, measures the freeboard and hence provides ice thicknesses with relative errors increasing with decreasing thickness, whereas SMOS' relative errors increase with increasing thickness (Kaleschke et al., 2010). A first validation of the synergistic SMOS/CryoSat-2 product was compared to the NASA Ice Bridge campaign in 2013 and clearly showed the improved skill of combined product (Kaleschke et al., 2015a). Insufficient knowledge about the snow cover is the largest uncertainty for the retrieval of ice thickness with CryoSat-2 (Ricker et al., 2015). SMOS may help to further reduce this uncertainty because the snow thickness can be estimated from the L-band brightness temperature (Maaß et al., 2013).

3.1.2. Soil moisture in near-real time

Most operational users over land, in particular in Numerical Weather Prediction and operational hydrology, require soil moisture information

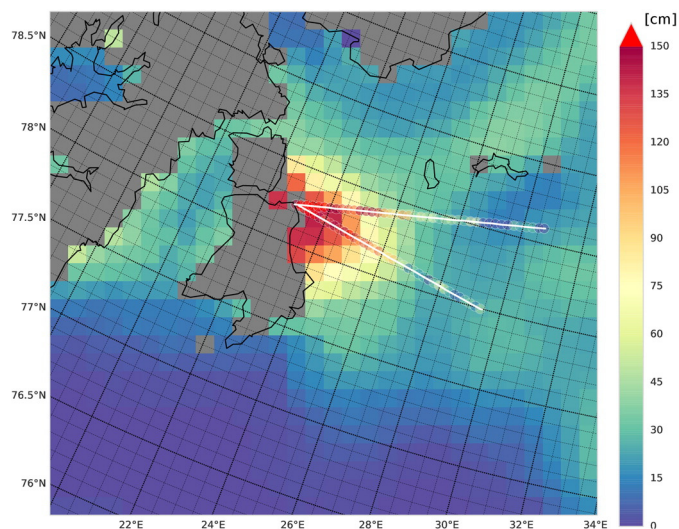


Fig. 7. SMOS sea ice thickness and airborne laser scanner (ALS) ice thickness (both in cm) on 24 March 2014 in the Barents Sea.
Credit: University of Hamburg, Alfred Wegener Institute, ESA.

to be available in near-real time, typically referring to less than 3 h after sensing. This requirement cannot be met with the operational level 2 processor due to the complexity of the geophysical retrieval algorithm and associated processing times. However, with 6 years of SMOS measurements available, statistical algorithms can be exploited to provide faster retrievals.

Neural networks are a promising technique to generate a SMOS based soil moisture product fulfilling the requirements of the operational communities: i) the data product is available in NRT, ii) it should display the same accuracy as the geophysical level 2 soil moisture data product, iii) the data should be retrieved over a maximum swath, and iv) the retrieval should rely on a minimum of auxiliary data files.

To test whether a statistical retrieval algorithm based on neural networks can meet these requirements, several neural network configurations using different combinations of input data sets (i.e. SMOS brightness temperatures, MODIS NDVI, C-band ASCAT backscattering coefficients, ECOCLIMAP soil texture maps, and ECMWF simulated soil temperature) and training data sets (i.e. soil moisture data from ECMWF's Integrated Forecast System (IFS) models, SMOS level 3 soil moisture data sets from the Centre Aval de Traitement des Données SMOS (CATDS)) were analysed (Rodríguez-Fernández et al., 2015a). The performance of the resulting neural network based soil moisture datasets was evaluated using in situ measurements from the U.S. Department of Agriculture (USDA) Soil Climate Analysis Network (SCAN) and it was found that the product quality is as good as, or even slightly better than, the actual quality of the global level 3 soil moisture data.

For the SMOS NRT soil moisture processor implemented operationally, (Rodríguez-Fernández et al., 2015b) the optimal input data set comprises SMOS NRT brightness temperatures in three incidence angle bins from 30 to 45° in 5° bins (for both H and V polarizations), soil temperature data from ECMWF and the maximum dynamic soil moisture range associated to the observed brightness temperatures at a given SMOS grid point. The training data for the neural network were extracted from the five-year SMOS level 2 soil moisture data set covering the period from 2010 to 2012. In addition, the global agreement with respect to the SMOS level 3 soil moisture has been evaluated. Fig. 8 shows the local temporal correlation of the SMOS soil moisture data in NRT with respect to the level 3 soil moisture dataset computed from June 2010 to June 2013. The blank areas are regions affected by RFI or with less than 30 points in the times series of collocated SMOS

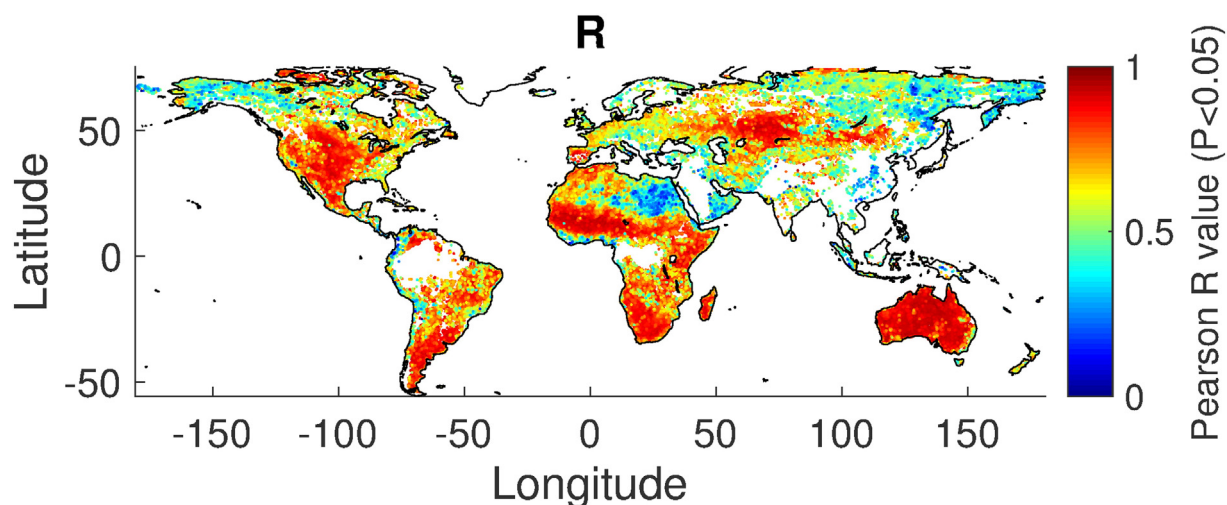


Fig. 8. Map of the local temporal correlation (Pearson R coefficient) between the SMOS NRT soil moisture data and the SMOS level 3 soil moisture data from CATDS. The blank areas are regions affected by RFI or with less than 30 points in the times series of collocated SMOS NRT and SMOS level 3 soil moisture due to snow, frozen soil or dense vegetation. Credit: CESBIO, ESA

NRT and SMOS level 3 soil moisture due to snow, frozen soil or dense vegetation. The two soil moisture datasets exhibit similar temporal dynamics. The lower temporal correlation is found in the northeast of Africa (a region known to be affected by RFI) and northern latitudes, where the Pearson correlation decreases to -0.5 . The temporal correlation over Australia, Africa, America and part of Europe is higher than 0.7 . First assessments indicate that this new soil moisture data product in NRT exhibits performances comparable or better than the level 2 soil moisture data product since the neural network performs a global statistical consistency analysis of the reference soil moisture dataset and thus excludes soil moisture estimates that are not consistent globally. The new NRT product is available from 2016 onwards and will be distributed through WMO's Global Telecommunication System (GTS) and EUMETSAT's EUMETCast in NetCDF format. The data quality will be routinely assessed and compared against the nominal level 2 and 3 products.

3.1.3. Severe winds

The measurement and prediction of surface wind speeds in Tropical Cyclones (TC) is of primary importance for storm intensification forecasting and land-fall risk mitigation. However, getting accurate direct or remote measurements over the ocean is still a very difficult and challenging task. Traditionally available surface wind speed products in Tropical Cyclones include the estimates from spaceborne scatterometers (e.g., ASCAT on Metop-A&B, OSCAT) and multi-frequency radiometer retrievals (WindSAT, AMSR-2, SSM/I), the airborne Step-Frequency Microwave Radiometer (SFMR) surface wind estimates (Uhlhorn et al., 2007) and the H*WIND analyses, available from NOAA, which objectively combine all available surface and near surface wind observations collected over a several hours' period from multiple platforms. With active remote methods of wind measurement saturating in hurricane force winds and generally suffering from rain contamination (Weissman et al., 2002), microwave radiometry has played an important and increasing role in recent years. SMOS brightness temperatures have been used to track severe winds based on the fact that in the microwave spectral region the emissivity from the sea surface increases with increased surface roughness and foam and thus with wind speed (Reul et al., 2012).

Upwelling radiation at L-band is significantly less affected by rain and atmospheric effects than at higher microwave frequencies, hence L-band measurements from SMOS mission offer a new unique opportunity to complement existing ocean satellite high wind observations in tropical cyclones and severe weather (Reul et al., 2012). An empirical

law was derived to describe the relation between the surface wind speed modulus and the difference of brightness temperature observed at a certain wind force and the brightness temperature observed for the smooth water surface (with the same physical parameters temperature and salinity). Using such a law for retrieving surface wind speed from SMOS data, the evolution of the SMOS retrieved maximum surface wind speed (Fig. 9) and the radii (from the storm eyes) of the domain where winds exceed 34, 50 and 64 knots were shown to be consistent with hurricane model solutions and observation analyses (Reul et al., 2012).

An extensive validation of SMOS retrieved wind speed has been performed (Reul et al., 2015b) using co-localised SFMR data and H*WIND products, both being used routinely as guidance for operational TC forecast and advisory products. Root mean square (rms) differences between SMOS retrieved winds and SFMR and H*WIND values is found to be in the order of $4\text{--}5$ m/s over the wind speed range $0\text{--}50$ m/s (averaged at SMOS ~ 50 km spatial resolution). This is comparable with Numerical Weather Prediction (NWP) product accuracy from e.g. ECMWF or NCEP-GFS at wind speed ranges below 33 m/s. However, the rms error and biases of NWP products strongly increase ($12\text{--}16$ m/s) when the wind speed exceeds hurricane force (Reul et al., 2015b) while SMOS winds still show an rms of ~ 5 m/s in those extreme conditions (Fig. 9).

To date a larger number of storms has been successfully tracked and current work in collaboration with the UK Met Office focuses on assessing the skill of SMOS data for severe wind forecasting using the entire SMOS archive. Future work focuses on exploiting the synergy between complementary measurements from multiple satellite instruments such as SMOS, SMAP and AMSR-2 to derive an optimised blended ocean surface wind product in extreme atmospheric conditions over the ocean, based on low-microwave frequency radiometer observations (Zabolotskikh et al., 2015; Reul et al., 2015b). A blended SMOS/AMSR-2 high wind speed products and database is currently generated in the frame of ESA's STSE SMOS + STORM project (<http://www.smosstorm.org/>). New measurements from the SMAP radiometer with a ~ 30 km ground resolution in brightness temperatures will complement the combined sampling of SMOS and AMSR-2 to derive an improved storm-tracking in extreme conditions from low-frequency microwave radiometers.

3.2. SMOS products and data assimilation

Any observation has a value in itself as a self-standing estimate of a geophysical parameter at the supported spatial and temporal scales.

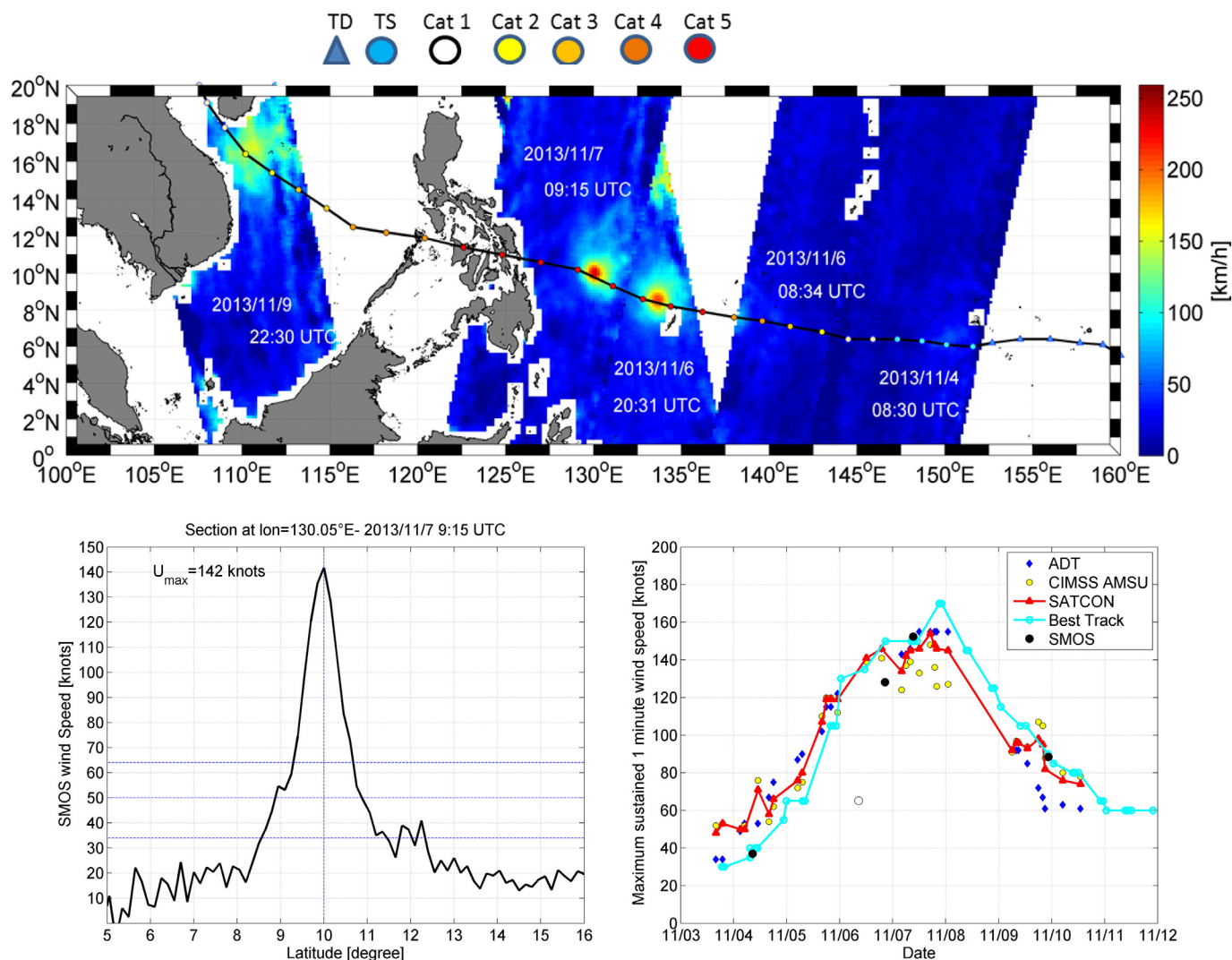


Fig. 9. Top: SMOS retrieved surface wind speed [km/h] along the eye track of super typhoon Haiyan from 4 to 9 Nov. 2013. Bottom left: North–south section through the SMOS retrieved wind speed field reaching 142 knots (~ 260 km/h) during the Haiyan Typhoon passage on 7 Nov. 2013 at 09:15 UTC. Bottom Right: Maximum sustained 1 min wind speed estimated during the Haiyan typhoon. SMOS data (black filled dots) compared to estimates made available by the Cooperative Institute for Meteorological Satellite Studies (CIMSS, see <http://tropic.ssec.wisc.edu/>): Advanced Dvorak Technique (ADT = blue diamond), CIMSS (yellow filled dots), CIMSS Satellite Consensus (SATCON) product (red) and Best Track from the National Hurricane Centre (NHC) (cyan). Note the empty circle corresponds to the SMOS measurements for the 6 November (am) for which only a small portion of the cyclone signal was intercepted. Maximum 10 min wind speed deduced from the SMOS algorithm was multiplied by 1/0.93, adopting the conversion factor proposed in (Harper et al., 2010) between one min winds and 10 min winds. Symbols along the storm track represent intensity on the Saffir–Simpson scale. Tropical Depression (triangle), Tropical Storm to category 5 (coloured circles, see legend). (For interpretation of the references to colour in this figure legend, the reader is referred to the web version of this article.)
Credit: IFREMER, ESA.

When combined with other complementary measurements and a model based first guess, a physically consistent description of the current state of a system, i.e. analyses, can be derived together with a corresponding uncertainty estimate. Analyses are often used as initial conditions in forecasting systems and partly determine the predictive skill, particularly when we are facing initial value problems such as in weather forecasting. Integrating a novel type of measurement in forecasting systems poses big challenges – and opportunities – for operational users since the observation handling, the numerical model, and the data assimilation system require updates.

In applications related to land surface hydrology, soil moisture has often been treated as a weakly constrained so-called “sink-variable”. In Numerical Weather Prediction it is most important to get a correct estimate of the turbulent fluxes and subsequently screen level parameters and precipitation. In hydrology, the focus lies on an accurate description of rainfall–runoff relationships and carbon models are usually constrained by observations of atmospheric CO_2 measurements. None of these forecast systems were designed to provide accurate soil

moisture fields constrained by direct observations of surface soil moisture and substantial changes to the land model physics had to be made in a first step, e.g. the introduction of a new surface hydrology featuring a shallow top soil layer in the BETHY model (Scholze et al., 2015) or the use of improved and uniform soil data in the IFS (Balsamo et al., 2009).

Another common element is systematic differences between the models' first guess and the SMOS estimates caused by differences in vertical sampling. For most applications over land the water content in the root zone is most important since it influences evapotranspiration and therefore the exchange of water, energy, and carbon between the terrestrial surface and the atmosphere. In contrast, the SMOS-based moisture estimates represent the uppermost centimetres (up to 5 cm) of the soil only. Advanced land surface modules comprise several layers for the root zone and through the appropriate choice of model and observation errors in the data assimilation procedure some of the differences between model and observation are being taken into account. However, some systematic differences persist and an efficient minimization

through bias correction schemes is mandatory (e.g. Drusch et al., 2005, Verhoest et al., 2015).

After thorough data quality control and bias correction the impact of the SMOS observations on the soil moisture analyses were positive in the different applications. At ECMWF the analyses were based on screen level parameters, namely air temperature and relative humidity at 2 m and SMOS brightness temperatures (Munoz-Sabater, personal communication), whereas in Lievens et al. (2015, 2014) the impact of both, brightness temperatures and SMOS derived surface soil moisture, was quantified. For the assimilation experiments using the BETHY model (Scholze et al., 2015) spatially and temporally aggregated soil moisture estimates were used together with measurements of atmospheric CO₂ concentrations. Independently of the SMOS data sets used - brightness temperature or soil moisture products - the resulting analysed soil moisture fields were more accurate than the open loop model predictions when compared against the different independent validation data sets. The impacts on the forecast parameters, i.e. atmospheric temperatures and humidity, streamflow and net ecosystem exchange were neutral to slightly positive in most cases (Munoz-Sabater personal communication, Lievens et al., 2015, Scholze et al., 2015).

Two main conclusions can be drawn from these results related to land surface hydrology: (1) SMOS observations are of high quality and improve the soil moisture analyses used as initial conditions in forecasting systems. Although these models are designed towards very specific forecasting applications and already have high forecast skill the additional observational constraint does not deteriorate the forecast of associated forecast parameters. (2) To make optimal use of the improved initial soil moisture conditions, model physics including parameterisations and auxiliary data sets need to be adjusted. Assimilating new types of observations is therefore a consistent and elegant way to identify shortcomings in our process understanding and modelling.

In polar regions, uncertainties in sea ice thickness have been identified as an important factor potentially limiting the skill of seasonal forecasts of Arctic sea ice extent (Chevallier & Salas-Melia, 2012) and low-level atmospheric parameters, namely 2 m air temperature (Day et al., 2014). Potentially, the SMOS derived ice thickness data (Kaleschke et al., 2012; Tian-Kunze et al., 2014) can contribute to an improved description of the initial conditions and subsequently to an improved forecast. Experiments with the Massachusetts Institute of Technology general circulation model and a localised Singular Evolutive Interpolated Kalman filter showed that the assimilation of SMOS derived ice thickness data led to improved ice thickness forecasts when compared against independent observations; sea ice concentration forecasts were also found to be more accurate, although the overall improvement was smaller (Yang et al., 2014). It is foreseen to use the sea ice thickness estimates also in ECMWF's IFS and, in parallel, the assimilation of multi-frequency brightness temperatures rather than geophysical ice products is being prepared. One of the core tasks is therefore the implementation of a coupled ocean–ice–atmosphere model that can deliver input parameters for the radiative transfer model. The observation handling will benefit from the technical developments implemented for the soil moisture analysis.

Over the ocean, sea surface salinity (Martin, 2015; Köhl et al., 2014, Vinogradova et al., 2014, Hackert et al., 2014) and hurricane wind speed (Reul et al., 2015b) data have the potential to increase predictive skill on the seasonal and short- to medium-range forecast range, respectively.

SMOS has pioneered our ability to observe sea surface salinity globally and in a timely fashion on various spatial and temporal scales. Observed salinity patterns and geophysical features comprise basin wide salinity maxima and minima centres (Hernandez et al., 2014; Alory et al., 2012, Hasson et al., 2013), tropical instability waves (Yin et al., 2014), eddy transport of salt across major current boundaries (Reul et al., 2014a; Kolodziejczyk et al., 2015), large scale salinity anomalies associated to inter-annual climate variability (Durand et al., 2013 Hasson et al., 2014), surface signatures of equatorial upwelling (Alory et al., 2012; Maes et al., 2014), surface freshwater plume interactions

with tropical cyclones (Grotsky et al., 2012; Reul et al., 2014b) and excessive river runoff (Hopkins et al., 2013; Fournier et al., 2015). For the SMOS mission lifetime a comprehensive hurricane wind speed database was generated for exploitation at the UK Met Office and ECMWF. Both centres use wind measurements from various observation systems operationally and the integration of SMOS derived wind speeds is rather straightforward complementing the existing data. Both products have reached a level of maturity that allows the respective communities to start the integration in complex data assimilation systems.

As the next step, a forward operator will be integrated allowing the computation of model based brightness temperatures at the top of the atmosphere and routine data monitoring over the oceans. This is a mandatory task prior to data assimilation to identify any systematic or spurious differences between model and observations. It is assumed that the systematic differences in vertical and horizontal resolution between the SMOS measurements, other observations (e.g. Argo floats), and the uppermost model layer will need to be corrected for. Again, we assume that some developments for the soil moisture analysis can be adapted to ocean applications.

3.3. Future land products

SMOS data have been used extensively over land to derive additional higher-level products such as drought indices, root zone soil moisture, or evapotranspiration estimates (Martens et al., 2015). In this section we describe data sets based on SMOS brightness temperatures that are sufficiently mature for full exploitation in the 2016–2017 time frame.

3.3.1. Vegetation

In addition to surface soil moisture (being used as input for the SMOS drought index, an important monitoring and prediction tool for plant available water), SMOS provides observations on vegetation optical depth (Fig. 10), being simultaneously retrieved in the level 2 algorithm over land, following the so-called tau-omega (τ - ω) approach (Mo et al., 1982, Kerr & Njoku, 1990, Wigneron et al., 2007; Kerr et al., 2012). Both parameters aid agricultural applications such as crop growth, yield forecasting and drought monitoring, and provide input for carbon and land surface modelling. The level 2 dataset includes each retrieved parameter value together with the associated retrieval uncertainty.

Vegetation optical depth derived by passive microwave observations is determined by the water content, structure and density of the canopy (Kiriyashev et al., 1979). Vegetation water content is a key parameter in plant photosynthesis and transpiration and can be used to assess plant water stress, thus monitoring plant health. Furthermore, the sensitivity of vegetation optical depth to physical properties of the canopy, such as structure and density, is used to globally estimate aboveground biomass (Liu et al., 2015; Rahmoune et al., 2014), providing crucial input for climate change studies.

Given the potential SMOS has to improve our understanding of the global carbon cycle, current efforts focus on improving the SMOS level 2 retrievals over vegetated areas. The current processor version (v6) includes an improved land classification and representation of forested areas (Rahmoune et al., 2013), leading to an increased vegetation optical depth coverage over forested areas globally (Ferrazzoli et al., 2015).

Assimilating SMOS surface soil moisture into a carbon assimilation scheme built around a terrestrial biosphere model was found to improve global CO₂ flux estimates (Scholze et al., 2015). Similarly, assimilating SMOS surface soil moisture and AMSR-E derived vegetation optical depth into an evapotranspiration model was found to improve latent heat flux estimates over Australia (Martens et al., 2015).

Future work will concentrate on improving the retrieval algorithm for vegetation optical depth, verified by in-situ data. SMOS aims to provide estimates of vegetation water content with an accuracy of 0.5 kg m⁻² every six days (Kerr et al., 2001a). Global land surface

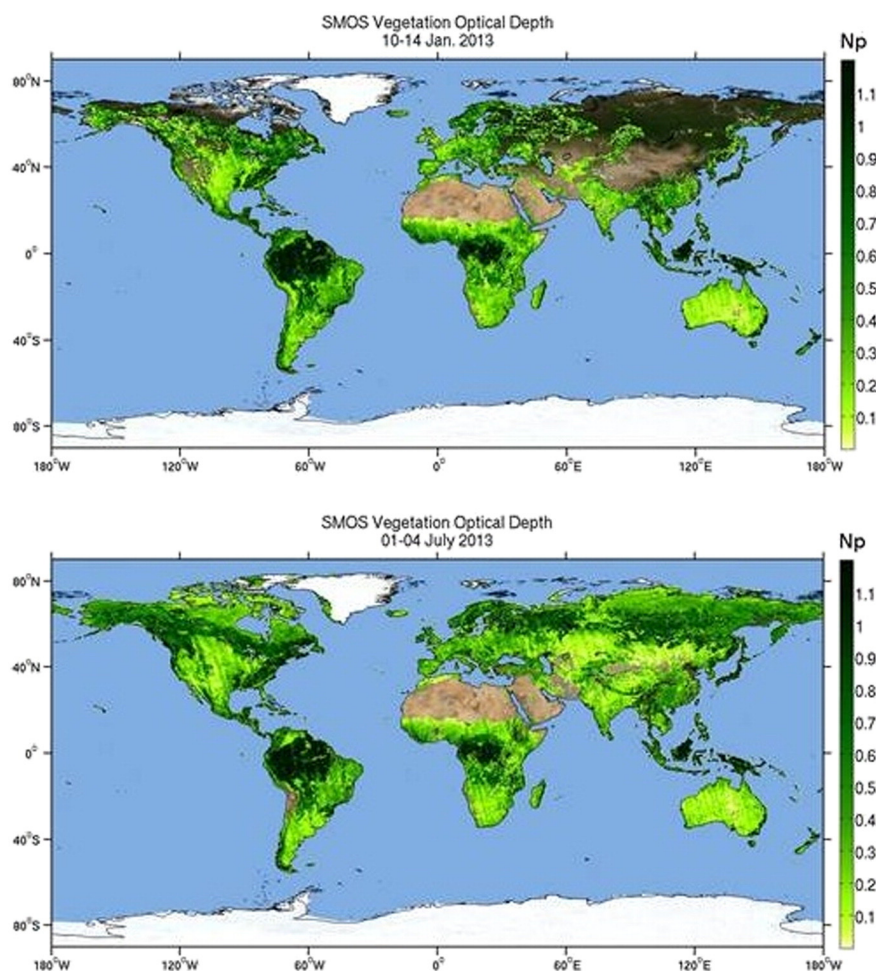


Fig. 10. Monthly vegetation optical depth derived from SMOS data for January (left) and July (right) 2013. Seasonal differences in vegetation are well visible. Credit: CESBIO, ESA.

models will need to be adapted to be able to assimilate both SMOS surface soil moisture and vegetation optical depth, and provide new products related to global carbon, energy and water budgets.

3.3.2. Soil freezing

The freeze/thaw state of the soil has a significant impact on the exchange of energy, water, and carbon between the land surface and the atmosphere. Given that more than half of the total landmasses of the Earth are affected by soil freezing, information about soil freeze and thaw state are important (Rautiainen et al., 2014).

An empirical change detection algorithm has been developed to detect seasonal soil freezing processes (Rautiainen et al., 2014, 2015). The algorithm is based on 3 years of brightness temperatures from a ground based L-band radiometer located at a forest test site in Finland and in-situ observations, such as soil frost tube observations and soil temperature. Compared to active sensors operating at higher frequencies, L-band offers an all-weather tool with a higher revisit time and, most importantly, a higher permittivity of water in solid and liquid states, being important for the characterisation of soils in transition between freeze and thaw state. The algorithm was subsequently tested at an open wetland site giving a first indication on whether it would be transferable to other soil types and applicable globally. Current work focuses on adapting the algorithm to space borne L-band brightness temperatures from SMOS and NASA's SMAP missions, with the aim to provide a global freeze-thaw product in the future.

Schwank et al. (2015) found that different snow densities could be distinguished and propagation effects must be taken into account in dry snow whilst running a study to determine the potential to retrieve dry-snow density and ground permittivity from multi-angular L-band brightness temperatures. Retrievals using SMOS data seem to underestimate actual ground permittivity by typically 30% as dry snow is wrongly considered as 'invisible.' Validation experiments still need to be conducted but these results are a step towards fully exploiting L-band brightness temperatures over cold regions of the Northern Hemisphere.

4. Summary and outlook

After 6 years in orbit the SMOS mission is in excellent technical condition, providing high quality data products to the scientific and operational community. The mission operations have been extended to 2017 by both ESA and CNES, jointly operating the SMOS mission. No technical limitations exist to extend the mission even beyond 2017. The instrument performance fulfils the requirements. The RFI contamination has been significantly improved in Europe and the Americas but remains a constraint in Asia and the Middle East. The mission's objectives have been reached over land and are being approached over ocean. Being an Earth Explorer mission, SMOS has delivered a vast amount of new science that has been leading to societal benefits across a wide range of disciplines.

Over oceans, SMOS has proven capabilities to detect mesoscale sea surface salinity features (scales <300 km) not resolved by in situ

observation networks (e.g. Argo floats) and provides a new interfacial measurement of sea surface salinity (within the top first centimetres of the ocean) that no global in situ observing system can sample. These two characteristics are a key scientific outcome of the mission over ocean, with applications in domains such as ocean circulation, oceanic freshwater cycle and bio-chemistry.

Over land, SMOS has been providing the most direct observations of soil moisture at an unprecedented accuracy for areas not contaminated by RFI. This information is used to monitor flood and drought events and supports the risk assessment during severe storms with associated heavy rainfall. For the generation of long term data records using different observation types it is expected that SMOS measurements can be used as a yardstick. Future products over land will include vegetation optical depth, aiding agricultural applications and food security, and a soil freeze product, contributing to the quantification of latent heat fluxes. Both these products will further our understanding of the carbon and land surface modelling.

SMOS observations have shown great potential for operational applications and data products continue to evolve. Three new products have been introduced, namely i) sea ice thickness, important for ship routing but also for climate research, ii) soil moisture in near-real time based on a statistical approach, providing valuable input data and appropriate timeliness for hydrological applications, and iii) severe winds, improving the forecast of severe storms.

SMOS data products are currently assimilated and used in forecasting systems, with activities over land being more advanced than over ocean. Besides the actual scientific process understanding, assimilating a novel type of observation in forecasting systems also requires of operational users an improved understanding of how to handle the observations, the numerical model and the data assimilation system. Over land, assimilating SMOS derived information has shown to have a positive impact on applications such as NWP, stream flow forecasting and the analysis of net ecosystem exchange. Assimilating SMOS derived sea ice thickness can potentially contribute to an improved characterisation of initial conditions for seasonal forecasts of Arctic sea ice extent and hence to an improved forecast. Over ocean, both sea surface salinity and severe wind speed have the potential to increase the predictive skill on the seasonal and short- to medium-range forecast range. The accompanying developments of the data assimilation systems and models are progressing well and the impact of SMOS observations will be quantified in the mission extension phase.

The extension of the SMOS mission operations beyond the original mission life not only provides an environment for continuous provision of observation data sets, which is an important prerequisite for developing (pre-) operational applications and establishing their use with operational users. The extension also opens the opportunity for using SMOS data in a climate research context. After 6 years in orbit inter-annual changes over land and ocean can now be seen which have the potential to provide additional capabilities to the activities of the Copernicus Climate Change core service in future and the climate discussion in general. Hence the achievements and continuous operations of the SMOS mission correspond directly to the new direction laid out in the “Earth Observation Science Strategy for ESA” (http://esamultimedia.esa.int/multimedia/publications/SP-1329_1/offline/download.pdf) emphasising continuity in data provision, stressing the importance of Earth Observation data for societal benefits and branching into new scientific areas such as vegetation and carbon.

The successful translation of scientific advances based on SMOS data into operational applications as well as the relevance of such observations for long-term climate research calls for an extension of such observations into the future, as recently voiced by the scientific and operational community at the 2nd SMOS conference in May 2015. In 2014, the International Space Science Institute (ISSI) facilitated an international expert forum focussing on the “Continuity of microwave observations in L-band for operational and climate applications”. Clear

statements were made as to the need of continuity in L-band observations beyond the current fleet of available missions. The recent loss of NASA's Aquarius mission in June 2015 and the loss of the radar on NASA's SMAP mission in July 2015 has further emphasised the need for forward planning towards an L-band follow-on mission in an international context.

Acknowledgements

The authors would like to express their thanks to the various scientific and industrial teams involved in the development and operations of the SMOS mission for their valuable contributions. Lars Kaleschke thanks the Cluster of Excellence ‘CiSAP’ (EXC177), University of Hamburg and the German Science Foundation (DFG) for funding. Yann Kerr and Nicolas Reul thank the CNES programmes TOSCA (Terre Océan Surface Continentales Atmosphère) and CATDS for their continuous support. Nicolas Reul thanks ESA for funding his work under the STSE SMOS + Storms project.

References

- Al Bitar, A., Kerr, Y. H., Merlin, O., Cabot, F., & Wigneron, J. -P. (2013). Global Drought Index from SMOS Soil Moisture. *Proceedings of 2013 International Geoscience and Remote Sensing Symposium IGARSS*.
- Alory, G., Maes, C., Delcroix, T., Reul, N., & Illig, S. (2012). Seasonal dynamics of sea surface salinity off Panama: The far Eastern Pacific Fresh Pool. *Journal of Geophysical Research*, 117, C04028. <http://dx.doi.org/10.1029/2011JC007802>.
- Al-Yaari, A., Wigneron, J. -P., Kerr, Y., De Jeu, R., Ducharne, A., Rodriguez-Fernandez, N., ... Dolman, A. J. (2015). Testing regression equations to derive long-term global soil moisture datasets from passive microwave observations. *This RSE Special Issue (in press)*.
- Anterrieu, E. (2011). On the detection and quantification of RFI in L1a signals provided by SMOS. *IEEE Transactions on Geoscience and Remote Sensing*, 49(10), 3986–3992. <http://dx.doi.org/10.1109/TGRS.2011.2136350>.
- Anterrieu, E., Khazaal, A., Cabot, F., & Kerr, Y. (2015). Geolocation of RFI sources with sub-kilometric accuracy from SMOS interferometric data. *This RSE Special Issue (under review)*.
- Balsamo, G., Viterbo, P., Beljaars, A., van der Hurk, B., Hirschi, M., Betts, A., & Scipal, K. (2009). A revised hydrology for the ECMWF model: Verification from field site to terrestrial water storage and impact in the integrated forecast system. *Journal of Hydrometeorology*, 10. <http://dx.doi.org/10.1175/2008JHM1068.1>.
- Boutin, J., Martin, N., Yin, X., Reul, N., & Spurgeon, P. (2012). First assessment of SMOS measurements over open ocean: Part II sea surface salinity. *IEEE Transactions on Geoscience and Remote Sensing*, 50(5), 1662–1675.
- Brown, M. E., Escobar, V., Moran, S., Entekhabi, D., O'Neill, P. E., Njoku, E. G., Doorn, B., & Entin, J. K. (2013). NASA's Soil Moisture Active Passive (SMAP) mission and opportunities for applications users. *Bulletin of the American Meteorological Society*, 94, 1125–1128. <http://dx.doi.org/10.1175/BAMS-D-11-00049.1>.
- Chevallier, M., & Salas-Melia, D. (2012). The role of sea ice thickness distribution in the Arctic sea ice potential predictability: A diagnostic approach with a coupled GCM. *Journal of Climate*, 25(8), 3025–3038. <http://dx.doi.org/10.1175/JCLI-D-11-00209.1>.
- Daganzo-Eusebio, E., Oliva, R., Kerr, Y. H., Nieto, S., Richaume, P., & Mecklenburg, S. M. (2013). SMOS radiometer in the 1400–1427-MHz passive band: Impact of the RFI environment and approach to its mitigation and cancellation. *IEEE Transactions on Geoscience and Remote Sensing*, 51(10), 4999–5007.
- Day, J. J., Hawkins, E., & Tietche, S. (2014). Will Arctic sea ice thickness initialization improve seasonal forecast skill? *Geophysical Research Letters*, 41, 7566–7575. <http://dx.doi.org/10.1002/2014GL061694>.
- De Rosnay, P., Drusch, M., Boone, A., Balsamo, G., Decharme, B., Harris, P., ... Wigneron, J. -P. (2009). The AMMA land surface model intercomparison experiment coupled to the community microwave emission model: ALMIP-MEM. *Journal of Geophysical Research*, 114. <http://dx.doi.org/10.1029/2008JD010724>.
- De Rosnay, P., Sabater, J. M., Albergel, C., Dutra, E., Drusch, M., Isaksen, L., ... Kerr, Y. (2015). Evaluation of CMEM microwave emission modelling configurations for SMOS brightness temperature observations and associated multi-year global L-band brightness temperature re-analysis. *Quarterly Journal of the Royal Meteorological Society (in preparation)*.
- Dorigo, W. A., Xaver, A., Vreugdenhil, M., Gruber, A., Hegyiová, A., Sanchis-Dufau, A. D., ... Drusch, M. (2013). Global automated quality control of in situ soil moisture data from the international soil moisture network. *Vadose Zone Journal*, 12(3). <http://dx.doi.org/10.2136/vzj2012.0097>.
- Drusch, M., Wood, E. F., & Gao, H. (2005). Observation operators for the direct assimilation of TRMM microwave imager retrieved soil moisture. *Geophysical Research Letters*, 32, L15403. <http://dx.doi.org/10.1029/2005GL023623>.
- Drusch, M., Holmes, T., De Rosnay, P., & Balsamo, G. (2009). Comparing ERA-40 based L-band brightness temperatures with Skylab observations: A calibration/validation study using the community microwave emission model. *Journal of Hydrometeorology*, 10. <http://dx.doi.org/10.1175/2008JHM964.1>.
- Durand, F., Alory, G., Dussin, R., & Reul, N. (2013). SMOS reveals the signature of Indian Ocean dipole events. *Ocean Dynamics*, 63(11–12), 1203–1212.

- Entekhabi, D., Njoku, E., O'Neill, P., Kellogg, K., & Entin, J. (2011). The NASA Soil Moisture Active Passive (SMAP) mission formulation. *Proceedings of 2011 International Geoscience and Remote Sensing Symposium (IGARSS)*.
- Ferrazzoli, P., Vittucci, C., Kerr, Y., Richaume, P., Guerriero, L., & Vaglio Laurin, G. (2015). SMOS retrieval over forests: Exploitation of optical depth and validation of soil moisture. *This RSE Special Issue* (under review).
- Font, J., Camps, A., Borges, A., Martín-Neira, M., Boutin, J., Reul, N., ... Mecklenburg, S. (2010). SMOS: The challenging sea surface salinity measurement from space. *Proceedings of the IEEE*, 98, 649–665.
- Font, J., Boutin, J., Reul, N., Spurregeer, P., Ballabrera-Poy, J., Chuprin, A., ... Delwart, S. (2013). SMOS first data analysis for sea surface salinity determination. *International Journal of Remote Sensing*, 34(9–10), 3654–3670.
- Fournier, S., Chapron, B., Salisbury, J., Vandemark, D., & Reul, N. (2015). Comparison of spaceborne measurements of sea surface salinity and colored detrital matter in the Amazon plume. *Journal of Geophysical Research, Oceans*, 120, 3177–3192. <http://dx.doi.org/10.1002/2014JC010109>.
- Gaillard, F. (2012). ISAS-Tool version 6: Method and configuration. Available from: <http://archimer.ifremer.fr/doc/00115/22583/>.
- Grodsky, S. A., Reul, N., Lagerloef, G., Reverdin, G., Carton, J. A., Chapron, B., ... Kao, H. -Y. (2012). Haline hurricane wake in the Amazon/Orinoco plume: AQUARIUS/SACD and SMOS observations. *Geophysical Research Letters*, 39, L20603. <http://dx.doi.org/10.1029/2012GL053355>.
- Hackert, E., Ballabrera-Poy, J., Busalacchi, A. J., Zhang, R. -H., & Murtugudde, R. (2014). Impact of Aquarius sea surface salinity observations on coupled forecasts for the tropical Indo-Pacific Ocean. *Journal of Geophysical Research*, 119(7), 4045–4067.
- Harper, B. A., Keprt, J. D., & Ginger, J. D. (2010). Guidelines for converting for different wind speed averaging periods in tropical cyclone conditions. *World Meteorological Organization report, WMO/TD no.1555* (August 2010).
- Hasson, A., Delcroix, T., & Boutin, J. (2013). Formation and variability of the South Pacific Sea Surface Salinity maximum in recent decades. *Journal of Geophysical Research, Oceans*, 118(10), 5109–5116. <http://dx.doi.org/10.1002/jgrc.20367>.
- Hasson, A., Delcroix, T., Boutin, J., Dussin, R., & Ballabrera-Poy, J. (2014). Analyzing the 2010–2011 La Niña signature in the tropical Pacific sea surface salinity using in situ data, SMOS observations, and a numerical simulation. *Journal of Geophysical Research, Oceans*, 119(6), 3855–3867.
- Hernandez, O., Boutin, J., Kolodziejczyk, N., Reverdin, G., Martin, N., Gaillard, F., ... Vergely, J. L. (2014). SMOS salinity in the subtropical North Atlantic salinity maximum: 1. Comparison with Aquarius and in situ salinity. *Journal of Geophysical Research, Oceans*, 119, 8878–8896.
- Hopkins, J., Lucas, M., Dufau, C., Sutton, M., Stum, J., Laurent, O., & Channelliere, C. (2013). Detection and variability of the Congo River plume from satellite derived sea surface temperature, salinity, ocean colour and sea level. *Remote Sensing of Environment*, 139, 365–385. <http://dx.doi.org/10.1016/j.rse.2013.08.015>.
- Kaleschke, L., Maaß, N., Haas, C., Hendricks, S., Heygster, G., & Tonboe, R. T. (2010). A sea ice thickness retrieval model for 1.4 GHz radiometry and application to airborne measurements over low salinity sea-ice. *The Cryosphere*, 4, 583–592. <http://dx.doi.org/10.5194/tc-4-583-2010>.
- Kaleschke, L., Tian-Kunze, X., Maass, N., Mäkynen, M., & Drusch, M. (2012). Sea ice thickness retrieval from SMOS brightness temperatures during the Arctic freeze-up period. *Geophysical Research Letters*, 39, L05501. <http://dx.doi.org/10.1029/2012GL05916>.
- Kaleschke, L., Tian-Kunze, X., Maaß, N., Ricker, R., Hendricks, S., & Drusch, M. (2015a). Improved retrieval of sea ice thickness from SMOS and Cryosat-2. *Proceedings of 2015 International Geoscience and Remote Sensing Symposium IGARSS*. <http://goo.gl/WSdoQD>
- Kaleschke, L., Tian-Kunze, X., Maaß, N., Beitsch, A., Wernecke, A., Miernecki, M., ... Casal, T. (2015b). SMOS sea ice product: Operational application and validation in the Barents Sea marginal ice zone. *This RSE Special Issue* (under review).
- Kerr, Y. H., & Njoku, E. G. (1990). A semi empirical model for interpreting microwave emission from semi-arid land surfaces as seen from space. *IEEE Transactions on Geoscience and Remote Sensing*, 28(3), 384–393.
- Kerr, Y. H., Waldteufel, P., Wigneron, J. -P., Martinuzzi, J. M., Font, J., & Berger, M. (2001a). Soil moisture retrieval from space: The Soil Moisture and Ocean Salinity (SMOS) mission. *IEEE Transactions on Geoscience and Remote Sensing*, 39(8), 1729–1735.
- Kerr, Y.H., Waldteufel, P. & Berger, M. (2001b). Mission objectives and scientific requirements of the Soil Moisture and Ocean Salinity (SMOS) mission. Noordwijk (NL), ESA-ESTEC. Available from http://earth.esa.int/pub/ESA_DOC/SMOS003.pdf.
- Kerr, Y. H., Waldteufel, P., Wigneron, J. -P., Delwart, S., Cabot, F., Boutin, J., ... Mecklenburg, S. (2010). The SMOS mission: New tool for monitoring key elements of the global water cycle. *Proceedings of the IEEE*, 98(5), 666–687.
- Kerr, Y. H., Waldteufel, P., Richaume, P., Wigneron, J. -P., Ferrazzoli, P., Mahmoodi, A., ... Delwart, S. (2012). The SMOS soil moisture retrieval algorithm. *IEEE Transactions on Geoscience and Remote Sensing*, 50(5), 1384–1403.
- Kerr, Y. H., Al-Yaari, A., Rodriguez-Fernandez, N., Parrons, M., Molerio, B., Leroux, D., Bircher, S., Mahmoodi, A., Mialon, A., Richaume, P., Delwart, S., Al Bitar, A., Pellarin, T., Bindlish, R., Jackson, T. J., Rudiger, C., Waldteufel, P., Mecklenburg, S., & Wigneron, J. -P. (2015). Overview of SMOS performance in terms of global soil moisture monitoring after six years in operation. *This RSE Special Issue* (under review).
- Kirdyashev, K. P., Chukhlantsev, A. A., & Shutko, A. M. (1979). Microwave radiation of the earth's surface in the presence of vegetation cover. *Radiotekhnika i Elektronika*, 24, 256–264.
- Köhl, A., Sena Martins, M., & Stammer, D. (2014). Impact of assimilating surface salinity from SMOS on ocean circulation estimates. *Journal of Geophysical Research, Oceans*, 119, 5449–5464. <http://dx.doi.org/10.1002/2014JC010040>.
- Kolodziejczyk, N., Hernandez, O., Boutin, J., & Reverdin, G. (2015). SMOS salinity in the subtropical North Atlantic salinity maximum: 2. Two-dimensional horizontal thermohaline variability. *Journal of Geophysical Research, Oceans*, 120, 972–987. <http://dx.doi.org/10.1002/2014JC010103>.
- Lagerloef, G., Yueh, S., & Piepmeyer, J. (2013). NASA's Aquarius mission provides new ocean view. *Sea Technology*, 54(1), 26–29.
- Le Vine, D. M., Dinnat, E. P., Lagerloef, G. S. E., de Mattheis, P., Abraham, S., Utku, C., & Kao, H. (2014). Aquarius: Status and recent results. *Radio Science*, 49(9), 709–720.
- Lievens, H., Kumar Tomer, S., Al Bitar, A., De Lannoy, G. J. M., Drusch, M., Dumedah, G., ... Pauwels, V. R. N. (2014). SMOS soil moisture assimilation for improved hydrologic simulation in the Murray Darling Basin, Australia. *Remote Sensing of Environment*, 168, 146–162.
- Lievens, H., De Lannoy, G. J. M., Al Bitar, A., Drusch, M., Dumedah, G., Hendricks Franssen, H. -J., ... Pauwels, V. R. N. (2015). Assimilation of SMOS soil moisture and brightness temperature products into a land surface model. *This RSE Special Issue* (in press).
- Liu, Y. Y., Van Dijk, A. I. J. M., De Jeu, R. A. M., Canadell, J. G., McCabe, M. F., Evans, J. P., & Wang, G. (2015). Recent reversal in loss of global terrestrial biomass. *Nature Climate Change*. <http://dx.doi.org/10.1038/NCLIMATE2581>.
- Maaß, N., Kaleschke, L., Tian-Kunze, X., & Drusch, M. (2013). Snow thickness retrieval over thick Arctic sea ice using SMOS satellite data. *The Cryosphere*, 7, 1971–1989. <http://dx.doi.org/10.5194/tc-7-1971-2013>.
- Maaß, N., Kaleschke, L., Tian-Kunze, X., Mäkynen, M., Drusch, M., Krumpfen, T., Hendricks, S., Lensu, M., Haapala, J. & Haas, C. (2015). Validation of SMOS sea ice thickness retrieval in the northern Baltic Sea. *Tellus A*, 67, doi: <http://dx.doi.org/http://dx.doi.org/10.3402/tellusa.v67.24617>.
- Macelloni, G., Pampaloni, P., Brogioni, M., Cagnati, A., & Drinkwater, M. (2006). DOMEX 2004: And experimental campaign at Dome-C Antarctica for the calibration of space-borne low-frequency microwave radiometers. *IEEE Transactions on Geoscience and Remote Sensing*, 44(10), 2642–2653.
- Macelloni, G., Brogioni, M., Pampaloni, P., & Cagnati, A. (2007). Multi-frequency microwave emission from the East Antarctic Plateau: Temporal and spatial variability. *IEEE Transactions on Geoscience and Remote Sensing*, 43, 2029–2039.
- Macelloni, G., Brogioni, M., & Rahmoune, R. (2012). Characterisation of the spatial and temporal stability of the East Antarctic plateau in the low-microwave bands. *MicroRad, 12th Specialist meeting*.
- Macelloni, G., Brogioni, M., Pettinato, S., Zasso, R., Crepaz, A., Zaccaria, J., & Drinkwater, M. (2013). Ground based L-band emission measurements at DOME-C Antarctica: The DOMEX-2 experiment. *IEEE Transactions on Geoscience and Remote Sensing*, 51(9), 4718–4730. <http://dx.doi.org/10.1109/TGRS.2013.2277921>.
- Macelloni, G., Brogioni, M., Aksoy, M., Johnson, J. T., Jezek, K. C., & Drinkwater, M. R. (2014). Understanding SMOS Data in Antarctica. *Proceedings of 2014 International Geoscience and Remote Sensing Symposium IGARSS*.
- Maes, C., Reul, N., Behringer, D., & O'Kane, T. (2014). The salinity signature of the equatorial Pacific cold tongue as revealed by the satellite SMOS mission. *Geoscience Letters*, 1(1), 1–7.
- Martens, B., Miralles, D. G., Lievens, H., Fernandez-Prieto, D., & Verhoest, N. E. C. (2015). Improving terrestrial evaporation estimates over continental Australia through assimilation of SMOS soil moisture. *International Journal of Applied Earth Observation and Geoinformation*. <http://dx.doi.org/10.1016/j.jag.2015.09.012>.
- Martin, M. (2015). Suitability of satellite sea surface salinity data for assessing and correcting ocean forecasts. *This RSE Special Issue* (under review).
- Martin-Neira, M., Corbella, I., Torres, F., Durán, I., Duffo, N., Kainulainen, J., ... Suess, M. (2015). SMOS instrument performance and calibration after 5 years in orbit. *This RSE Special Issue* (under review).
- McMullan, K., Brown, M., Martin-Neira, M., Rits, W., Ekholm, S., Marti, J., & Lemnarczyk, J. (2008). SMOS: The payload. *IEEE Transactions on Geoscience and Remote Sensing*, 46, 594–605.
- Mecklenburg, S., Drusch, M., Kerr, Y. H., Font, J., Martin-Neira, M., Delwart, S., ... Crapolicchio, R. (2012). ESA's Soil Moisture and Ocean Salinity mission: Mission performance and operations. *IEEE Transactions on Geoscience and Remote Sensing*, 50(5), 0196–2892.
- Mo, T., Choudhury, B. J., Schmutge, T. J., Wang, J. R., & Jackson, T. J. (1982). A model for microwave emission from vegetation-covered fields. *Journal of Geophysical Research*, 7(C13), 11229–11237.
- Oliva, R., Daganzo, E., Kerr, Y., Mecklenburg, S., Nieto, S., Richaume, P., & Gruhier, C. (2012a). SMOS radio frequency interference scenario: Status and actions taken to improve the RFI environment in the 1400–1427 MHz passive band. *IEEE Transactions on Geoscience and Remote Sensing*, 50(5), 1427–1439.
- Oliva, R., Nieto, S., & Felix, F. (2013). RFI detection algorithm: Accurate geolocation of the interfering sources in SMOS images. *IEEE Transactions on Geoscience and Remote Sensing*, 51(10), 4993–4998.
- Oliva, R., Daganzo, E., Soldo, Y., Kerr, Y., Cabot, F., Richaume, P., ... Lopes, G. (2015). Status of SMOS RFI in the 1400–1427 MHz passive band after 5 years of mission. *This RSE Special Issue* (under review).
- Picard, G., Brucker, L., Fily, M., Gallée, H., & Krinner, G. (2009). Modeling time series of microwave brightness temperature in Antarctica. *Journal of Glaciology*, 55(191), 537–551.
- Rahmoune, R., Ferrazzoli, P., Kerr, Y., & Richaume, P. (2013). SMOS level 2 retrieval algorithm over forests: Description and generation of global maps. *IEEE Journal of Selected Topics in Applied Earth Observations and Remote Sensing*, 6(3), 1430–1439.
- Rahmoune, R., Ferrazzoli, P., Singh, Y. K., Kerr, Y., Richaume, P., & Al Bitar, A. (2014). SMOS retrieval results over forests: Comparisons with independent measurements. *IEEE Journal of Selected Topics in Applied Earth Observations and Remote Sensing*, 7(9), 3858–3866.
- Rautiainen, K., Lemmetyinen, J., Schwank, M., Kontu, A., Ménard, C., Mätzler, C., ... Pulliainen, J. (2014). Detection of soil freezing from L-band passive microwave observations. *Remote Sensing of Environment*, 147, 206–218.

- Rautiainen, K., Parkkinen, T., Lemmetyinen, J., Schwank, M., Wiesmann, A., Ikonen, J., ... Pulliainen, J. (2015). SMOS prototype algorithm for detecting autumn soil freezing. *This RSE Special Issue* (under review).
- Reul, N., Tenerelli, J., Chapron, B., Vandermark, D., Quilfen, Y., & Kerr, Y. (2012). SMOS satellite L-band radiometer: A new capability for ocean surface remote sensing in hurricanes. *Journal of Geophysical Research*, 117. <http://dx.doi.org/10.1029/2011JC007474>.
- Reul, N., Chapron, B., Lee, T., Donlon, C., Boutin, J., & Alory, G. (2014a). Sea surface salinity structure of the meandering Gulf Stream revealed by SMOS sensor. *Geophysical Research Letters*, 41, 3141–3148. <http://dx.doi.org/10.1002/2014GL059215>.
- Reul, N., Quilfen, Y., Chapron, B., Fournier, S., Kudryavtsev, V., & Sabia, R. (2014b). Multisensor observations of the Amazon–Orinoco river plume interactions with hurricanes. *Journal of Geophysical Research, Oceans*, 119, 8271–8295. <http://dx.doi.org/10.1002/2014JC010107>.
- Reul, N., Font, J., Boutin, J., Turiel, A., Tenerelli, J., Yin, X., ... Mecklenburg, S. (2015a). An overview of 5 years of SMOS salinity data. *This RSE Special Issue* (under review).
- Reul, N., Chapron, B., Collard, F., Cotton, J., Francis, P., Zabolotskikh, E., & Donlon, C. (2015b). A revised L-band radio-brightness sensitivity to extreme winds under tropical cyclones: The 5 years SMOS-storm database. *This RSE Special Issue* (under review).
- Ricker, R., Hendricks, S., Perovich, D. K., Helm, V., & Gerdes, R. (2015). Impact of snow accumulation on CryoSat-2 range retrievals over Arctic sea ice: An observational approach with buoy data. *Geophysical Research Letters*, 42, 4447–4455. <http://dx.doi.org/10.1002/2015GL064081>.
- Rodríguez-Fernández, N. J., Aires, F., Richaume, P., Kerr, Y. H., Prigent, C., Kolassa, J., ... Drusch, M. (2015a). Soil moisture retrieval using neural networks: Application to SMOS. *IEEE Transactions on Geoscience and Remote Sensing*, 53(11), 5991–6007. <http://dx.doi.org/10.1109/TGRS.2015.2430845>.
- Rodríguez-Fernández, N. J., Richaume, P., Muñoz-Sabater, J., De Rosnay, P., & Kerr, Y. H. (2015b). SMOS near-real-time soil moisture processor based in neural networks: Specifications CESBIO SMOS ground segment report SO-TN-CB-GS-038. CESBIO.
- Rodríguez-Fernández, N., Kerr, Y., Wigneron, J. -P., Al-Yaari, A., De Jeu, R. A. M., van der Schalie, R., ... Mecklenburg, S. (2015c). Eleven-years of an homogeneous soil moisture dataset from AMSR-E and SMOS observations. *Proceedings of 2015 International Geoscience and Remote Sensing Symposium IGARSS*.
- Scholze, M., Kaminski, T., Knorr, W., Blessing, S., Vossbeck, M., Grant, J. P., & Scipal, K. (2015). Simultaneous assimilation of SMOS soil moisture and atmospheric CO₂ in situ observations to constrain the global terrestrial carbon cycle. *This RSE Special Issue* (under review).
- Schwank, M., Matzler, C., Wiesmann, A., Wegmuller, U., Pulliainen, J., Lemmetyinen, J., ... Drusch, M. (2015). Snow density and ground permittivity retrieved from L-band radiometry: A synthetic analysis. *IEEE Journal of Selected Topics in Applied Earth Observations and Remote Sensing*, 8(8), 3833–3845. <http://dx.doi.org/10.1109/JSTARS.2015.2422998>.
- Skou, N., Kristensen, S. S., Sobjaerg, S. S., & Balling, J. (2015). Airborne L-band radiometer mapping of the Dome-C area in Antarctica. *IEEE Journal of Selected Topics in Applied Earth Observations and Remote Sensing*, 8(7), 3656–3664.
- Tian-Kunze, X., Kaleschke, L., Maass, N., Maekynen, M., Serra, N., & Drusch, M. (2014). SMOS derived sea ice thickness: Algorithm baseline, products specifications and initial verification. *The Cryosphere*, 8, 997–1018. <http://dx.doi.org/10.5194/tc-8-997-2014>.
- Uhlhorn, E. W., Black, P. G., Franklin, J. L., Goodberlet, M., Carswell, J., & Goldstein, A. S. (2007). Hurricane surface wind measurements from an operational stepped frequency microwave radiometer. *Monthly Weather Review*, 135(9), 3070–3085.
- Van der Schalie, R., Kerr, Y., Wigneron, J. -P., Al-Yaari, A., & De Jeu, R. A. M. (2015). Global SMOS soil moisture retrievals from the land parameter retrieval model. *International Journal of Applied Earth Observation and Geoinformation* (in press). 10.1016/j.jag.2015.08.005.
- Vergely, J. -L., Waldteufel, P., Boutin, J., Yin, X., Spurgeon, P., & Delwart, S. (2014). New total electron content retrieval improves SMOS sea surface salinity. *Journal of Geophysical Research, Oceans*, 119(10), 7295–7307. <http://dx.doi.org/10.1002/2014JC010150>.
- Verhoest, N. E. C., van den Berg, M. J., Martens, B., Lievens, H., Wood, E. F., Pan, M., ... Pauwels, V. R. N. (2015). Copula-based downscaling of SMOS soil moisture with implicit bias correction for application in a land surface model. *IEEE Transactions on Geoscience and Remote Sensing*, 53(6), 3507–3521.
- Vinogradova, N. T., Ponte, R. M., Fukumori, I., & Wang, O. (2014). Estimating satellite salinity errors for assimilation of Aquarius and SMOS data into climate models. *Journal of Geophysical Research, Oceans*, 119, 4732–4744. <http://dx.doi.org/10.1002/2014JC009906>.
- Weissman, D. E., Bourassa, M. A., & Tongue, J. (2002). Effects of rain rate and wind magnitude on sea winds scatterometer wind speed errors. *Journal of Atmospheric and Oceanic Technology*, 19, 738–746.
- Wigneron, J. -P., Kerr, Y. H., Waldteufel, P., Saleh, K., Escorihuela, M. -J., Richaume, P., ... Schwank, M. (2007). L-band microwave emission of the biosphere (L-MEB) model: Description and calibration against experimental data sets over crop fields. *Remote Sensing of Environment*, 107(4), 639–655.
- Yang, Q., Losa, S. N., Losch, M., Tian-Kunze, X., Nerger, L., Liu, J., ... Zhang, Z. (2014). Assimilating SMOS sea ice thickness into a coupled ice-ocean model using a local SEIK filter. *Journal of Geophysical Research, Oceans*, 119. <http://dx.doi.org/10.1002/2014JC009963>.
- Yin, X., Boutin, J., Reverdin, G., Lee, T., Arnault, S., & Martin, N. (2014). SMOS sea surface salinity signals of tropical instability waves. *Journal of Geophysical Research, Oceans*, 119, 7811–7826. <http://dx.doi.org/10.1002/2014JC009960>.
- Zabolotskikh, E., Mitnik, L. M., Reul, N., & Chapron, B. (2015). New possibilities for geophysical parameter retrievals opened by GCOM-W1 AMSR2. *IEEE Journal of Selected Topics in Applied Earth Observations and Remote Sensing*, PP(99), 1–14.